Chem Soc Rev

Quantum state resolved gas-surface reaction dynamics experiments: A tutorial review

Journal:	*Chemical Society Reviews*
Manuscript ID:	CS-REV-06-2015-000476.R1
Article Type:	Tutorial Review
Date Submitted by the Author:	15-Jul-2015
Complete List of Authors:	Chadwick, Helen; Ecole Polytechnique Federale de Lausanne, Chemistry Beck, Rainer; Ecole Polytechnique Federale de Lausanne, Chemistry

Quantum state resolved gas-surface reaction dynamics experiments: A tutorial review

Helen Chadwick and Rainer D. Beck

Laboratoire de Chimie Physique Moléculaire,

Ecole Polytechnique Fédérale de Lausanne, Switzerland.

Key Learning Points:

1. How to prepare beams of quantum state selected molecules through rapid adiabatic passage.
2. Physisorption *vs* chemisorption.
3. What is state and mode specificity?
4. What is vibrational bond selectivity?
5. Orientation *vs* alignment and alignment dependent reactivity.

Abstract:

We present a tutorial review of our quantum state resolved experiments designed to study gas-surface reaction dynamics. The combination of a molecular beam, state specific reactant preparation by infrared laser pumping, and ultrahigh vacuum surface analysis techniques make it possible to study chemical reactivity at the gas-surface interface in unprecedented detail. We describe the experimental techniques used for state specific reactant preparation and for detection of surface bound reaction products developed in our laboratory. Using the example of the reaction of methane on Ni and Pt surfaces, we show how state resolved experiments uncovered clear evidence for vibrational mode specificity and bond selectivity, as well as steric effects in chemisorption reactions. The state resolved experimental data provides valuable benchmarks for comparison with theoretical models for gas-surface reactivity aiding in the development of a detailed microscopic understanding of chemical reactivity at the gas-surface interface.

1. Introduction

Chemical reactions that occur at the gas-surface interface play a central role both in important industrial processes, such as heterogeneous catalysis and molecular beam epitaxy, as well as in nature for example in atmospheric and interstellar chemistry. In all of these processes, the collision of a gas phase molecule with a solid surface can lead to one of several outcomes such as inelastic scattering, trapping followed by desorption, or molecular or dissociative adsorption. For example, a methane (CH_4) molecule incident on the surface of a nickel catalyst will decompose much more readily *via* a dissociative chemisorption reaction than in a bimolecular gas phase collision. The nascent dissociation products of methane remain adsorbed on the catalyst surface where they can further decompose and/or react with other species to form products that will desorb back into the gas phase. In this way, the role of a catalyst is to provide a low energy pathway from reactants to products without being consumed in the chemical reaction.

The research field of gas-surface reaction dynamics aims to understand the details of the reactive processes at the gas-surface interface on a fundamental microscopic level. Experiments which study collisions between gas molecules and surfaces are performed under highly controlled conditions by defining as many of the parameters of a collision as possible. These include the speed and angle of incidence of the gas phase molecule onto the surface, the initial electronic, vibrational and rotational state of the reactant molecule, as well as its alignment or orientation relative to the surface. Single crystal samples cut in a specific crystallographic orientation are used to have a well-defined surface structure, with different crystallographic orientations used to represent different possible adsorption sites on a catalyst. The surface is also prepared under ultrahigh vacuum conditions to maintain a clean surface before the start of each experiment. The experimental section describes in detail the techniques used to achieve the control over these parameters.

The quantum state specific reactivity data obtained from highly controlled gas-surface experiments provide important information on the chemical reaction dynamics for gas-surface reactions. For example, the observation of vibrational state specificity and bond selectivity in chemisorption reactions immediately excludes any statistical rate theories from a realistic description of the microscopic reaction process. Furthermore, the detailed state resolved reactivity data provides a valuable benchmark for testing the results of first principles calculations of gas-surface reactivity. They therefore help to develop a predictive understanding of chemical reactivity at the gas-surface interface which can then be used to aid in the design and optimisation of efficient heterogeneous catalysts.

This tutorial review will summarise and build on key concepts in recent reviews of interactions at the gas-surface interface[1-3]. The outline of the review is as follows. The first section introduces key concepts and definitions that are used when discussing gas-surface reaction dynamics. In the following section, the experimental techniques employed for gas-surface reactions are described and the methods used for detecting the surface bound products are discussed. Recent results for the interaction of methane with transition metal surfaces are then presented which highlight the non-statistical nature of gas-surface collisions.

Finally, the quantum state resolved reactivity data are compared to the results from theoretical calculations before the review is concluded with a summary and future outlook.

2. Gas-surface key concepts and definitions

After a collision with a surface the incident molecule can either stay (adsorb) on the surface, or be scattered back into the gas phase. Molecules can adsorb onto the surface in different ways, as shown schematically in Fig. 1. Firstly, the molecule can be trapped weakly on the surface through van der Waals forces. This is referred to as physisorption. Physisorbed molecules are trapped in a shallow potential energy well and usually remain mobile in the plane of the surface. For trapping to occur, the incident molecule must lose sufficient translational energy normal to the surface to prevent it from being scattered back into the gas phase. The translational energy (E_t) and the incident angle (Φ) dependence of the trapping probability can be described by the Baule model[4]. This considers the collision to take place between hard spheres, and assumes that the collision occurs between a single initially stationary and isolated atom in the surface and the molecule. The trapping probability is then related to the fraction of the incident 'normal' kinetic energy of the molecule ($E_t \cos^2\Phi$) that is transferred to the surface. It follows that the trapping probability decreases with increasing E_t and decreasing Φ, as more 'normal' energy needs to be transferred to the surface for the molecule to be trapped. However this model neglects the co-operative motion of the surface atoms and treats lattice vibrations (phonons) only approximately. Consequently, the Baule model provides only a qualitative description of the energy dependence of the trapping probability.

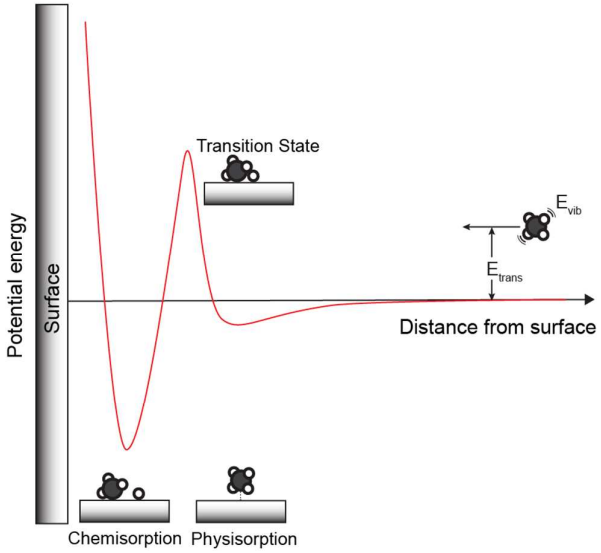

Fig. 1. A schematic one dimensional potential energy surface illustrating the adsorption of CH_4 on a transition metal surface. The depth of the physisorption well is exaggerated for clarity.

Another way in which the molecule can adsorb on the surface is through chemisorption, where a chemical bond is formed between the molecule and surface. Unlike physisorption, chemisorbed products are mostly immobile (except H-atoms) on the surface and bind to specific surface sites. The

probability that an incident molecule will undergo chemisorption is referred to as the sticking coefficient.

Molecular chemisorption occurs when a molecule remains intact upon adsorbing to the surface which is the case for CO chemisorption on a Pt(111) surface.

$C{\equiv}O(g) \rightarrow C{=}O(ads)$

It is also possible to break bonds within the molecule when it chemisorbs and make new bonds between the fragments and the surface. This is referred to as dissociative chemisorption. As bonds are being broken and formed, this is often an activated process where an energy barrier has to be overcome, as shown schematically in Fig. 1. For example, the dissociative chemisorption of methane on Ni(111) is a highly activated process with a barrier height on the order of 100 kJ/mol. The products of methane chemisorption are a chemisorbed methyl group and a chemisorbed hydrogen atom.

$CH_4(g) \rightarrow CH_3(ads) + H(ads)$

A molecule can become chemisorbed on a surface *via* different pathways. The first is that a molecule simply hits a vacant site (or sites) on the surface and has sufficient energy to overcome the activation barrier, and sticks to the surface. For this 'direct' chemisorption process the sticking coefficient increases with increasing E_t as more energy is available to overcome the activation barrier to chemisorption. Alternatively, the molecule can initially be trapped on the surface and chemisorb from this physisorbed 'precursor state'. This occurs if the trapped molecule finds a vacant site while moving across the surface and has enough energy to surmount the barrier between the physisorbed and chemisorbed state. This process is referred to as precursor mediated chemisorption, and is often characterised by an increase in sticking coefficient with decreasing E_t due to the increase in the initial trapping probability[5, 6].

3. Experimental techniques

3.1 Molecular beams

Molecular beams are an essential tool for chemical reaction dynamics experiments both for bimolecular reactions in the gas phase as well as gas-surface reactivity measurements since they enable the preparation of reactant species at high density with well-defined and controlled translational energy in a collision free environment.

A molecular beam is formed from a supersonic jet expansion. To create a supersonic expansion, the reactant gas is expanded from a stagnation pressure P_N and temperature T_N inside the nozzle through a small opening of diameter d into the high vacuum of the source chamber. Depending on the size of d compared to the mean free path λ at P_N and T_N either an effusive Knudsen flow ($\lambda > d$) or a supersonic expansion ($\lambda << d$) is formed. In a supersonic expansion, collisions between the molecules passing through the nozzle opening convert the random thermal motion inside the nozzle into directed flow with average speed

v of the jet expansion. Besides accelerating the molecules to v in the direction of the molecular beam, the collisions also cause strong translational and rotational cooling leading to a narrow speed distribution centered about v and the relaxation of the rotational population to the lowest rotational states. Assuming that this cooling is complete, the velocity of the molecular beam can be found using[7]

$$v = \sqrt{\frac{2k_b}{m}\left(\frac{\gamma}{\gamma-1}\right)T_N} \quad (1)$$

where m is the mass of the gas, γ is the ratio of the fixed pressure and fixed volume heat capacities (C_p/C_v) and T_N is the nozzle temperature. The velocity of the molecular beam can be controlled either by varying the nozzle temperature or by diluting, or seeding, the reactant in a carrier gas such as H_2 or He.

To create a molecular beam, the cold, fast core of the supersonic expansion is transmitted into a second, differentially pumped vacuum chamber by placing a 'skimmer' at a suitable distance from the nozzle. The skimmer is a streamlined aperture with very sharp edges to minimise backscattering of gas into the jet expansion. It also acts as a limiting conductance between the source chamber, which contains the nozzle, and the second pumping stage of the molecular beam source. This second stage often contains a chopper wheel which can be used to modulate the molecular beam and to generate short pulses for measuring its velocity distribution by the time-of-flight method. For this a quadrupole mass spectrometer, mounted on the molecular beam axis at a known distance from the chopper wheel, is used to measure the arrival time distribution of the molecule of interest. An example of such a distribution is shown in Fig. 2 for a pure CH_4 beam. With proper calibration, the experimental arrival time distribution can be transformed to either the velocity or the translational energy distribution of the reactants in the molecular beam.

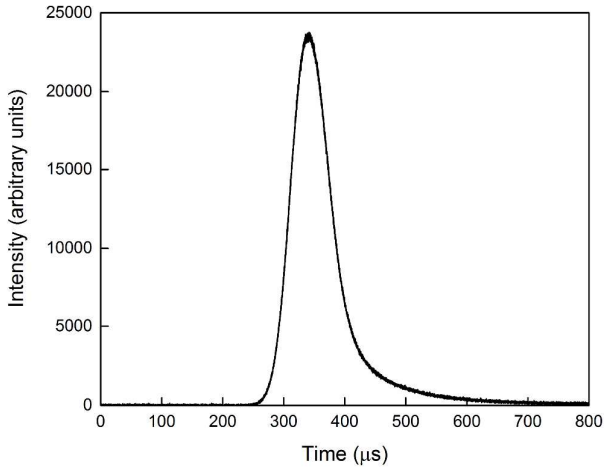

Fig. 2. The arrival time distribution from a time of flight measurement for a pure CH_4 molecular beam.

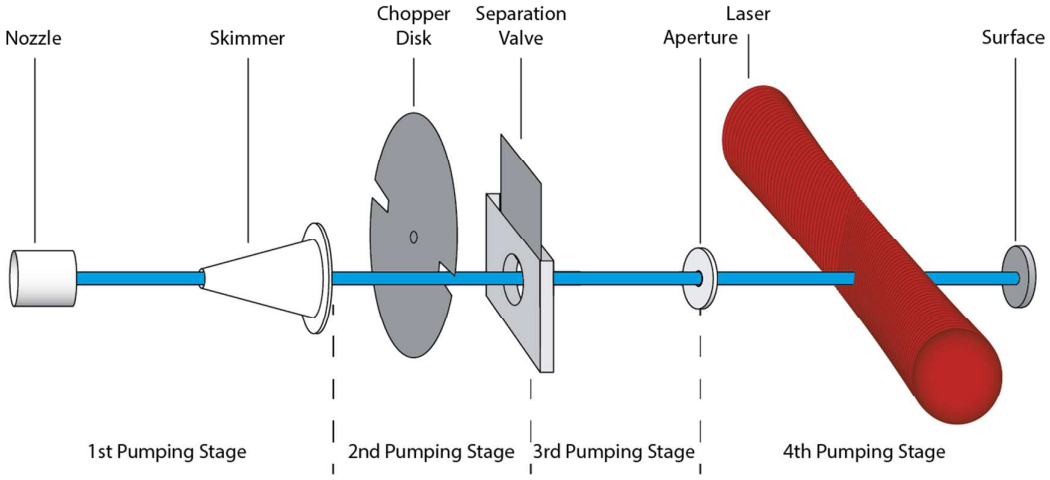

Fig. 3. A schematic overview of the molecular beam path of an apparatus used for a state resolved molecular beam/surface reactivity measurements.

After the chopper disk, the molecular beam enters a third pumping stage, which is used for collimation and to reduce the effusive gas load from the source chamber into the ultrahigh vacuum surface science chamber. A low profile separation valve is installed between the second and third stage to allow venting of the molecular beam source without breaking vacuum in the third and fourth chamber which require high temperature bakeout to achieve the ultrahigh vacuum conditions ($P< 10^{-10}$ mbar) needed to maintain a clean target surface. The molecular beam path is shown schematically in Fig. 3.

3.2 Reactant state preparation by infrared pumping

A molecular beam is an ideal environment for the quantum state specific preparation of reactant species in a specific rovibrational state by infrared (IR) pumping for several reasons:

1. The absence of Doppler broadening in the molecular beam results in narrow absorption lines of typically 1-3 MHz full width at half maximum matching the typical linewidth of single mode continuous wave laser sources for efficient IR pumping.

2. The rotational cooling of the jet expansion leaves only the lowest rotational energy levels of the reactant molecules populated again favouring optical state preparation methods that originate from a single rotational level of the vibrational ground state.

3. The collision free environment of the molecular beam permits state preparation by IR pumping far from the surface since typical lifetimes for spontaneous emission from rovibrationally excited states are on the millisecond timescale which is significantly longer than the typical flight time over a 10-100 mm distance to the surface.

4. The molecular beam creates a Doppler tuning effect for molecules passing through the curved wavefronts of the excitation laser beam which can be used for excitation by rapid adiabatic passage (RAP). RAP enables complete and robust population transfer from the initial to the final rovibrational quantum state.

It should be pointed out that the single mode IR lasers used here prepare the reactant molecules in a single vibrational eigenstate[8] which undergoes no intramolecular vibrational redistribution (IVR) as long as the molecule travels in molecular beam and is far (>1 nm) from the target surface. In the harmonic oscillator approximation, these eigenstates are identical with the normal modes ν_i of the molecule. For real molecules such as CH_4, anharmonicity can couple the normal modes for example *via* a stretch bend Fermi resonance which will cause the eigenstates to be a superposition of several normal modes. The molecule in the initially prepared eigenstate will still have no time dependence (IVR) but the prepared vibration can involve several normal modes. It is common to label the molecular eigenstates according to the dominant contribution of their expansion in a normal mode basis set. For example, strictly speaking the excited eigenstate of CH_4 labeled ν_1 contains only 95% ν_1 character and 2% $2\nu_2$ character plus other smaller contributions from other normal modes[9].

When the state prepared reactant molecule approaches the target surface, surface-induced IVR can start to occur because the eigenstates of the isolated molecules are not eigenstates of the combined molecule-surface system[8]. Whether this surface-induced IVR process can significantly change the reactant vibration before the reactive collision with the surface occurs depends on the strength of the molecule-surface interaction and the speed of the incident molecule.

3.2.1 Rabi-cycling versus Rapid adiabatic passage

Optical excitation with resonant coherent light will periodically move population between the initial and final state in a process called Rabi-cycling. The Rabi-cycling frequency Ω_R is given by

$$\Omega_R = \frac{\mu_{12} \cdot E}{\hbar} \qquad (2)$$

where μ_{12} is the transition dipole moment of the transition connecting the energy levels 1 and 2 and E the electric field strength of the excitation field. In nuclear magnetic resonance a so-called π-pulse is routinely used to invert the population of a two level nuclear spin system by a suitably tailored resonant radiofrequency pulse. This can be achieved because the system has a single Rabi-frequency, allowing all the population to be transferred under the same conditions as shown schematically by the blue line in Fig. 4. However, creating an optical π-pulse to invert the population of two rovibrational levels is generally not feasible for several reasons. First, the excitation laser field is often Gaussian, meaning different parts of the molecular beam are exposed to different electric field strengths leading to different Rabi-frequencies. Second, the distribution of speeds in the molecular beam means the molecules have different interaction times with the excitation field. Third, transitions between different degenerate *m*

levels for a given *J* have different transition dipole moments and so different Rabi-frequencies. In practice, these factors will lead to saturation of the two level system using Rabi-cycling averaged over many cycles of the different Rabi-frequencies and transfer only 50% of the population to the excited state as shown by the red line in Fig. 4, rather than complete inversion of the two level system with 100% excitation efficiency.

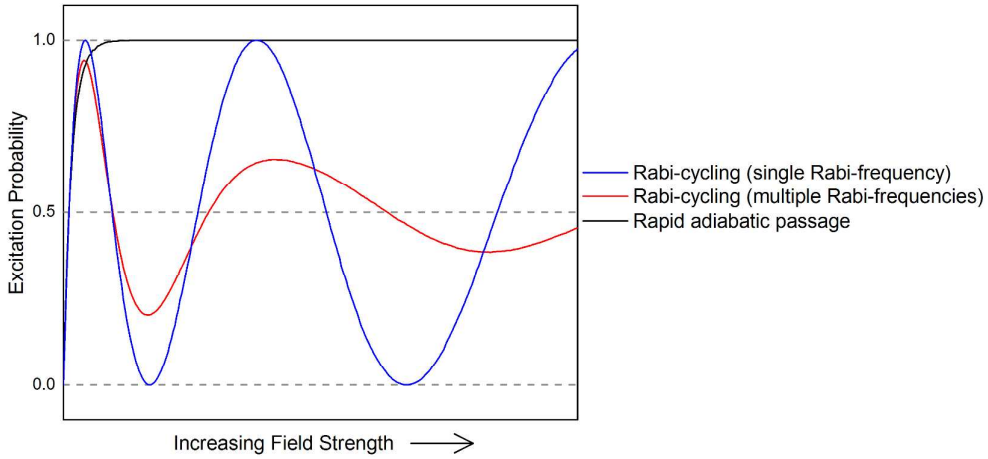

Fig. 4. The probability of exciting the molecules through Rabi-cycling, both for a single Rabi-frequency (blue line) and for several Rabi-frequencies (red line) and through rapid adiabatic passage (black line) as a function of the excitation field strength.

Alternatively, focusing the IR beam with a cylindrical lens in the direction of the molecular beam propagation creates a wavefront curvature for the electromagnetic field of the IR laser beam. Passage of the molecular beam through the curved wavefronts generates a Doppler tuning effect leading to a frequency sweep for the molecules passing through the IR beam. This frequency sweep can be adjusted *via* the wavefront curvature at the laser/molecular beam intersection by the choice of focal length for the cylindrical lens and the distance between the lens and the molecular beam. With proper focusing and sufficient IR power, complete population transfer is achieved by *rapid adiabatic passage* (RAP) between the initial and final rovibrational levels that are connected by the IR field, as shown by the black line in Fig. 4. One advantage of RAP is that it allows the inversion of a two level system independent of the precise conditions of laser intensity, molecular beam velocity, and Rabi-frequency as long as some basic conditions are satisfied. RAP therefore provides a robust excitation method that can be used to prepare intense beams of state specifically prepared molecules for reaction dynamics studies. For details see a recent publication from our group[10].

3.2.2 Double resonance excitation schemes

State preparation by double resonance excitation offers several advantages over single photon excitation. First, the combination of two single-photon IR excitation steps extends the accessible energy range for reactant vibrational excitation to both higher and lower energy compared to single laser excitation. With two IR optical parametric oscillator (OPO) systems that are each tunable over 2500-4000 cm^{-1}, it is possible to access vibrational levels in the

energy range from 0-8000 cm^{-1} using either scheme A or B illustrated in Fig. 5, which is significantly larger than the tuning range covered by a single OPO.

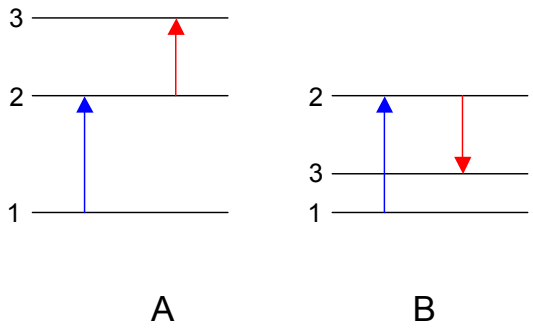

Fig. 5. Excitation schemes for double resonance excitation.

The laser power available from the IR OPO sources is sufficient to saturate both steps in a double resonance excitation scheme providing many more excited molecules than direct continuous wave laser pumping of weakly allowed overtone (Δv_i=2) transitions. Moreover, using stepwise excitation *via* RAP, complete population transfer from an initial level 1 to a final level 3 can be achieved as described in Ref.[10].

Furthermore, double resonance excitation enables the preparation of totally symmetric vibrational levels that cannot be accessed by a single photon transition from a totally symmetric vibrational ground state. For example, the $2\nu_3$ overtone of the infrared active antisymmetric C-H stretch normal mode ν_3 of CH_4 is split into three subcomponents of vibrational symmetry A_1, E, and F_2. Only the $2\nu_3(F_2)$ subcomponent is accessible by a single photon overtone transition from the totally symmetric (A_1) ground state but all three A_1, E, and F_2 subcomponents of $2\nu_3$ are accessible using double resonance excitation *via* the $\nu_3(F_2)$ level at 3019 cm^{-1}. Double resonance excitation has been used to study the effect of vibrational symmetry on the reactivity of CH_4 prepared in the three symmetry components A_1, E, and F_2[11].

3.2.3 State preparation *via* stimulated Raman pumping

Totally symmetric vibrations such as the symmetric C-H stretch fundamental ν_1 in CH_4 cannot be excited by single photon transitions. However, since ν_1 is Raman active it can be prepared using stimulated Raman pumping using two high power pulsed laser beams where their frequency difference matches the frequency of the Raman active vibrational mode. This can be represented by excitation scheme B shown in Fig. 5, where level 2 is a virtual level. The first, or pump laser excites to this intermediate level and the second, or Stokes laser transfers the molecules to the final excited state.

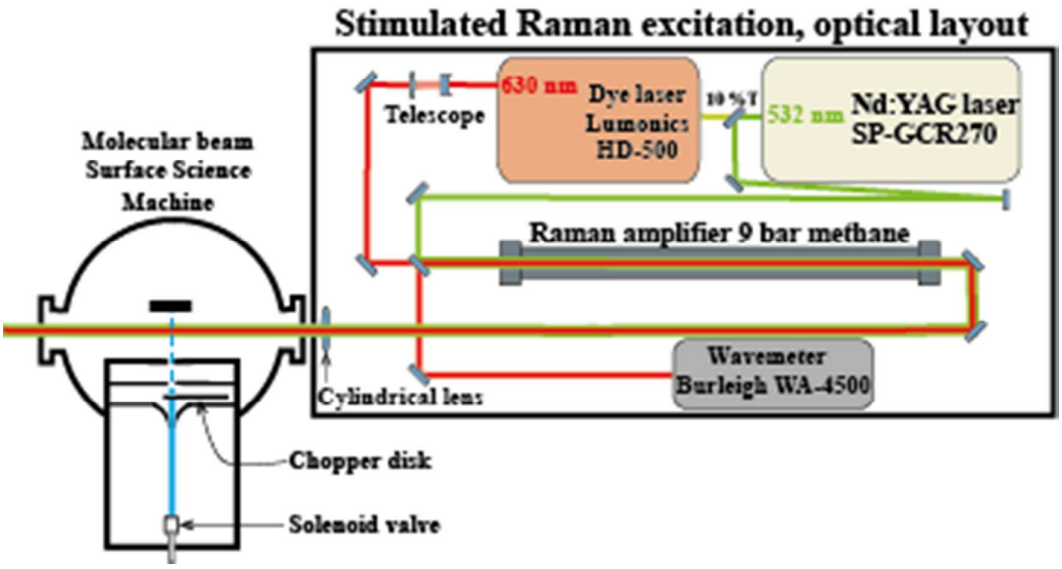

Fig. 6. Optical setup used for stimulated Raman pumping of CH_4 in the molecular beam.

The optical setup used for stimulated Raman pumping is shown schematically in Fig. 6. The 532 nm Raman pump beam is produced by generating the second harmonic of an injection-seeded, Nd:YAG laser operating at 20 Hz. The Stokes radiation at 630 nm is generated by a dye laser and amplified in a methane-filled Raman amplifier, both of which are pumped by the same Nd:YAG laser. To avoid beam instabilities resulting from thermal lensing inside the Raman amplifier, the methane is continuously circulated by a series of fans. The methane pressure of 9 bar in the Raman amplifier is chosen to tune the maximum of the gain profile to overlap the Q(0), Q(1), and Q(2) transitions used to excite the methane molecules in the molecular beam. Since the 0.05 cm^{-1} bandwidth of the Stokes radiation is insufficient to resolve these transitions, which have Raman shifts of 2916.47 cm^{-1}, 2916.49 cm^{-1} and 2916.53 cm^{-1} respectively, the analysis assumes that Raman excitation takes place simultaneously on all three transitions. The pump and Stokes laser beams were focused to a line parallel to the molecular beam by a cylindrical lens as shown in Fig. 7.

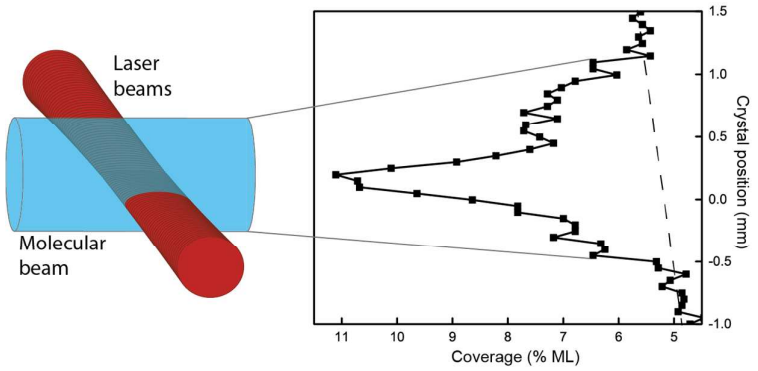

Fig. 7. Auger analysis (see section 3.3.2) of deposited carbon (right) together with a schematic of the excitation region (left).

The tight focusing of the laser beams within the molecular beam generates several distinct regions within this profile. The narrow peak in the center is due to the reaction of both laser excited ('laser-on') and unexcited ('laser-off') CH_4 molecules. The broad shoulders on either side of this peak represent the carbon footprint of the molecular beam due to chemisorption of unexcited CH_4. The carbon signal outside the molecular-beam footprint is due to carbon adsorbed from the background pressure in the chamber during the 90 min deposition time. The rise in the carbon baseline (illustrated by the dashed line) is due to the electron beam induced carbon formation during the 30 min Auger analysis. To obtain the amount of adsorbed carbon from laser-excited $CH_4(\nu_1)$, an extrapolated 'laser-off' baseline is subtracted from the central peak and the result integrated.

The analysis yields a state resolved reaction probability for $CH_4(\nu_1)$ up to an order of magnitude higher than that observed for preparation in the nearly iso-energetic antisymmetric C-H stretch mode ν_3[12]. Such mode specific reactivity will be discussed in more detail in section 4.1.

3.3 Product detection techniques

3.3.1 King and Wells beam reflectivity measurements

The molecular beam reflectivity method introduced by King and Wells (K&W) is a simple, self-calibrating method to measure the sticking probability of a molecule on a solid surface[13]. The method uses a mass spectrometer to monitor the partial pressure of the species of interest in the surface science chamber containing a clean surface sample for which the sticking coefficient is to be measured. A molecular beam is introduced into the chamber and initially scattered by an inert beam flag, which stops the molecular beam from reaching the surface sample. The pressure rise (P_1-P_0) caused by the scattered molecular beam is recorded by the mass spectrometer. At a certain time, the beam flag is removed from the molecular beam allowing it to scatter off the clean surface. If some of the molecules in the molecular beam stick on the surface, there will be a drop $\Delta P(t)$ in the corresponding partial pressure detected by the mass spectrometer. As the coverage of adsorbates on the surface increases, the pressure drop $\Delta P(t)$ will decrease with time. The beam flag is then shut at the end of the deposition and the scattered flux again monitored with the mass spectrometer, before the molecular beam is stopped from entering the chamber. A typical K&W trace measured for CH_4 on Pt(111) is presented in the left hand panel of Fig. 8.

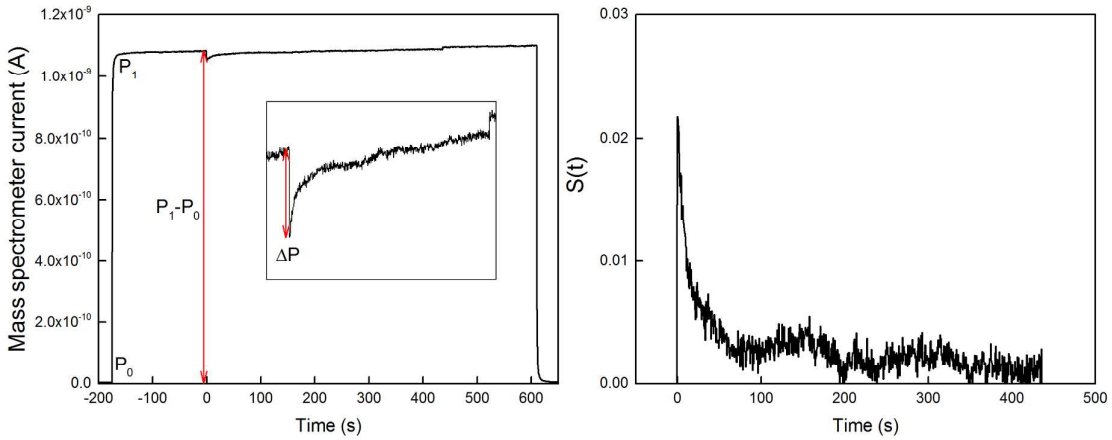

Fig. 8. King and Wells trace measured for CH_4 on Pt(111) at a surface temperature of 150 K (left) and the resulting time dependence of the sticking coefficient found using equation (3) (right).

The initial sticking coefficient S_0 on the clean surface can be directly calculated as

$$S_0 = \frac{\Delta P(t=0)}{P_1 - P_0} \qquad (3)$$

and the same expression can also be used to find the time dependence of the sticking coefficient, $S(t)$, as shown in the right hand panel of Fig. 8. By calibrating the mass spectrometer current against a pressure gauge for a pure CH_4 beam it is possible to determine the incident flux of methane molecules hitting the surface during the K&W measurements. This allows the incident dose to be found as the product of the flux and the time which can then be used with the time dependent sticking coefficient to find the sticking coefficient as a function of the surface coverage.

There are a few precautions that need to be taken to avoid artifacts that could cause systematic errors in a K&W measurements:

1. All of the molecules entering the surface science chamber need to hit the surface sample. While this seems trivial, it is possible that a fraction of the molecular beam is scattered by the entrance aperture causing them to miss the surface. Alternatively there might be an effusive beam from the differential pumping stages if the pressure is too high. These can both lead to an underestimation of the sticking coefficient.

2. Adsorbing on chamber walls or the cold surface manipulator can lead to a time dependent pumping speed for the molecule of interest. This will lead to a rising partial pressure P_1 even for constant molecular beam intensity which can complicate the analysis of the K&W traces.

3. Geometry effects: the relative position of the molecular beam flag, the surface sample, the mass spectrometer and the pumping port of the surface science chamber are important. A difference in detection efficiency for molecules scattered off the molecular beam flag compared to molecules scattered off the

surface sample can cause an offset (step) in the partial pressure measurement leading to a systematic error. This is especially important if very small sticking coefficients (S_0< 1%) are to be measured by the K&W method.

3.3.2 Auger electron spectroscopy

Auger electron spectroscopy (AES) is used to assess the cleanliness of sample surfaces before experiments and to quantify the adsorbate coverage on the surface after reactant deposition. This widely used surface science technique consists of detecting electrons emitted from core atomic orbitals (Auger electrons), as a consequence of the relaxation of the electronic configuration of the atom after a first core electron (primary electron) has been removed. The primary electron is ejected with an electron beam with an energy of between 1 and 5 keV. As the kinetic energy of the Auger electrons depends only on the electron energy level spacing of the parent atom, it is possible to unequivocally detect all atomic species other than hydrogen and helium. The sensitivity of the technique is limited to the first few atomic layers below the surface due to the finite elastic escape depth of the Auger electrons.

Auger spectra are often recorded as the derivative of the Auger electron current versus kinetic energy with a lock-in amplifier. Derivative spectra are obtained directly by applying a small amplitude modulation to the energy analyser and locking the amplifier to the modulation frequency. The amplitude of the modulation determines the resolution of the derivative spectrum. By convention, Auger intensities are measured as the absolute difference between the positive and negative peaks from the baseline in the derivative spectrum, and locations on the kinetic energy scale are read at the minimum of the negative peak. Typical examples of derivative Auger electron spectra obtained for carbon and nickel are shown in the left and right hand panels of Fig. 9 respectively[14].

To determine the adsorbate coverage, the ratio of the Auger intensity of the adsorbate peak and the surface peak is used. Taking the ratio reduces any errors in the measurement due to fluctuations in detection efficiency of the Auger electrons. For absolute quantification of the adsorbate coverage, it is necessary to calibrate this ratio using a self-limiting reaction which produces a known saturation coverage. For example ethylene can be used to calibrate the ratio for carbon on a Ni(100) surface as this produces a saturation coverage of 0.5 monolayers of carbon at a surface temperature of 475 K[15].

The C and Ni AES signals are measured at typically 50 points in a line scan across the surface following the molecular beam depositions. Fig. 10 shows the C/Ni AES signal ratio obtained from such a line scan across a Ni(100) surface following two methane depositions in two different positions on the surface. Two ‘footprints’ of the molecular beam can be clearly seen labelled spot 1 and spot 2.

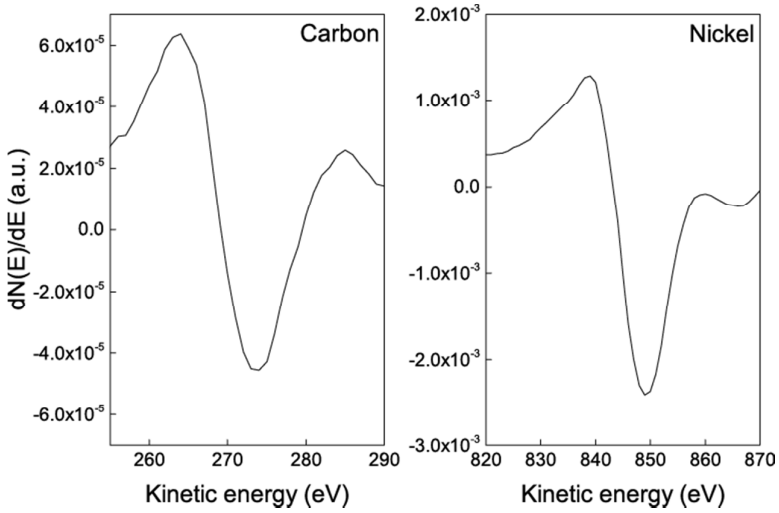

Fig. 9. Derivative Auger spectra for carbon (left) and nickel (right).

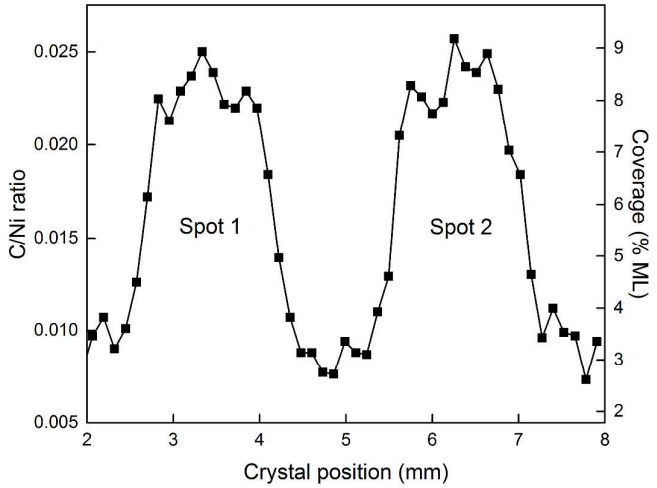

Fig. 10. Auger analysis of the surface carbon coverage following two identical depositions of CH_4 with an incident energy of 60 kJ/mol on a Ni(100) surface at a temperature of 475 K.

3.3.3 Reflection absorption infrared spectroscopy (RAIRS)

RAIRS is a surface sensitive vibrational spectroscopy technique that provides information about the structure of the adsorbed species on a reflective metal surface. For this, the metal surface is used as a mirror to reflect the incident IR beam on to a detector, as shown schematically in Fig. 11[16]. The adsorbates on the surface will absorb IR light when the frequency is in resonance with a vibrational transition, leading to a decrease in the detected infrared intensity. Taking the ratio of the spectrum measured during the molecular beam deposition with a background spectrum recorded before the start of the deposition for a clean surface produces the final RAIR spectrum. An example of a RAIR spectrum measured for the deposition of CH_4 on Pt(111) at a surface temperature of 150 K is shown in Fig. 12. The peak at 2883 cm^{-1} corresponds to the symmetric stretch of the CH_3(ads) and the 2754 cm^{-1} peak to a bend overtone.

Chen *et al.* have implemented RAIRS for state resolved surface reaction dynamics studies in order to probe for bond selectivity in the chemisorption of

partially deuterated methanes[17] (see section 4.2), an effect that could not be detected by AES. A further advantage of RAIRS over AES for product detection is that the weak IR light used in RAIRS does not affect the chemisorption process meaning it can be used to monitor the uptake of chemisorbed reaction products during the molecular beam deposition. In this way, the uptake of the chemisorption products can be recorded as a function of time in a single deposition experiment, which is not possible by AES since the high energy primary electron beam of the Auger spectrometer would interfere with the incident molecular beam by causing ionisation and fragmentation of the incident reactant. For this, RAIR spectra are simply recorded throughout the molecular beam deposition and the peak height (or area) of an absorption line is used as a measure of the surface coverage for a given adsorbate species. Calibration of the absorption peak height in terms of CH_3(ads) coverage was done with AES measurements following different exposure times or by simultaneous measurement of the sticking coefficient by the K&W method described above.

The time dependent RAIRS signal calibrated in terms of CH_3(ads) coverage together with the incident flux of CH_4 monitored from the partial pressure rise using a calibrated mass spectrometer allows the *uptake curve* for CH_3(ads) on Pt(111) to be obtained. The uptake curve gives the adsorbate coverage as a function of incident dose of the reactant species, an example of which is presented in Fig. 13. The coverage dependent sticking coefficient can then be obtained as the slope of the uptake curve which provides information whether the chemisorption is direct or precursor mediated.

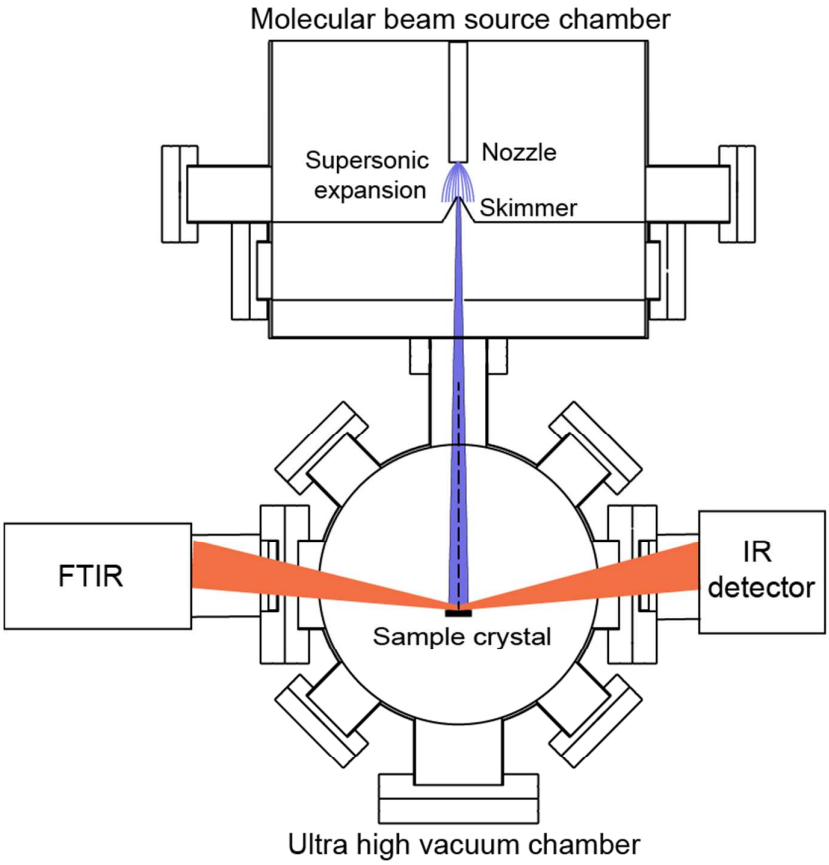

Fig. 11. A schematic overview of the surface science chamber used for RAIRS experiments.

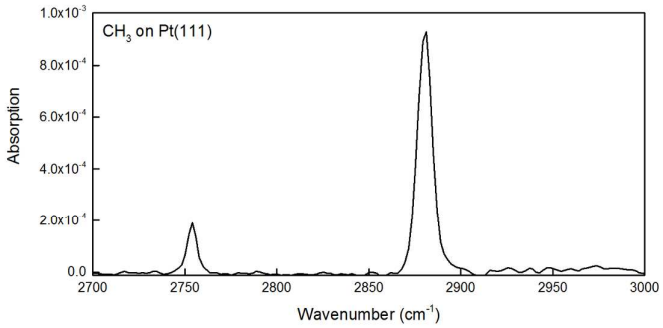

Fig. 12. A RAIR spectrum measured following the dissociative chemisorption of CH_4 on Pt(111) at a surface temperature of 150 K. The peaks at 2883 cm^{-1} and 2754 cm^{-1} correspond to the symmetric stretch and a bend overtone for CH_3(ads).

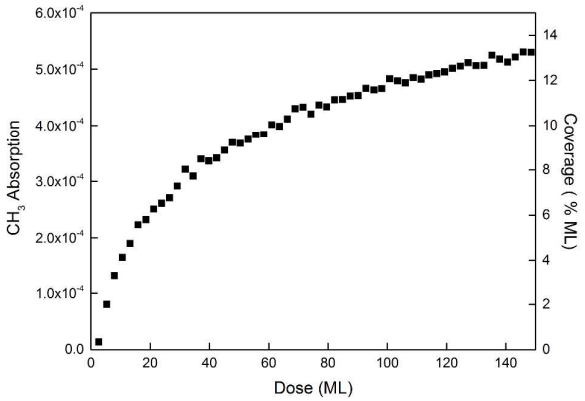

Fig. 13. A RAIRS uptake curve showing the peak height of the CH_3 absorption at 2883 cm^{-1} as a function of incident dose in monolayers (ML) where for Pt(111) 1 ML = $1.5x10^{15}$ atoms cm^{-2}.

Due to the surface selection rule for RAIRS, this technique only detects molecular vibrations with a component of their transition dipole moment directed along the surface normal. Vibrations for which the transition dipole moment lies in the plane of the surface cannot be detected by RAIRS. To maximise the RAIRS detection sensitivity, a near grazing angle of incidence (80±5°) is used for the IR light of the Fourier Transform Infrared (FTIR) spectrometer.

4. Results

4.1 Vibrational vs. translational activation of chemisorption and state specificity

For chemical reactions with an activation barrier, energy is needed for the reactants to overcome the barrier so that the products will form. This is why the reaction rates often increase exponentially with temperature as described by the Arrhenius equation for reactions occurring in thermal equilibrium . For the non-equilibrium conditions of a molecular beam, energy can be selectively added to any of the different degrees of freedom such as translation, rotation, vibration or electronic to study the effect on the reaction probability. Furthermore, for the vibrational excitation of a polyatomic molecule by a narrowband IR laser, it is possible to choose which of the vibrational modes are excited to probe for state specific effects.

Adding energy selectively to different degrees of freedom of the reactants and observing the effect on the reaction probability provides information about reaction dynamics and the potential energy surface (PES) for the reaction. Polanyi has proposed some simple rules which relate the energy consumption of a chemical reaction and the shape of the PES and verified them using molecular dynamics simulations[18]. For the reaction of an atom with a diatomic molecule (A + BC → AB + C) Polanyi distinguished two types of PES depending on the location of the transition state (top of the activation barrier), which separates reactants from products. These are shown schematically in Fig. 14. For a system with an early barrier, located in the entrance channel where the BC bond length has not yet been stretched, adding translational energy is more effective in increasing the reaction probability than adding the same amount of energy to vibration of BC. Conversely, on a PES with a late barrier, adding vibrational energy to BC is more efficient than translation because vibration corresponds to motion along the reaction co-ordinate.

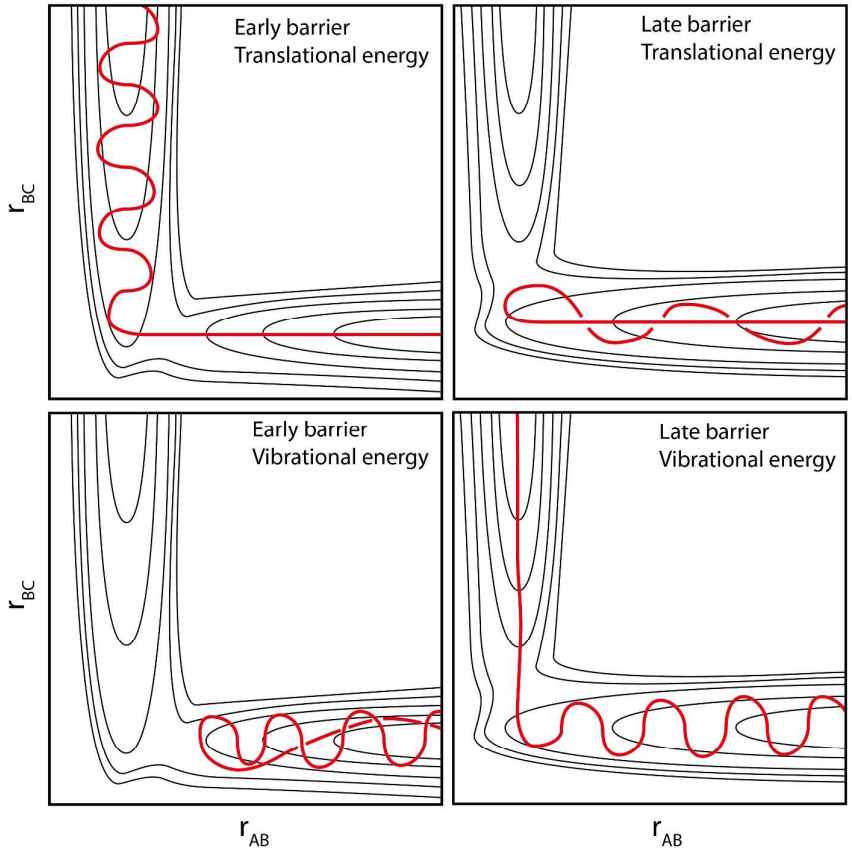

Fig. 14. Schematic potential energy surface for the A+BC→AB+C showing the effect of adding translational energy (top row) or vibrational energy (bottom row) to the incident BC if the reaction has an early barrier (left hand column) or late barrier (right hand column).

Polanyi's rules have been generalised to gas phase reactions of polyatomic molecules as well as to molecule-surface reactions. Reactions of polyatomic molecules with solid surfaces are inherently more complicated due to the presence of several vibrational modes. Excitation of different vibrational modes can affect the reactivity differently highlighting the multidimensionality

of the underlying PES. However, Polanyi's rules may still be applied qualitatively to reactions involving polyatomic molecules and surfaces.

The dissociative chemisorption of methane on transition metal surfaces such as Ni or Pt is a reaction with a large barrier and can be promoted through the addition of translational and/or vibrational energy. Seeded molecular beam experiments have been used by many groups to explore how the dissociative sticking coefficient ($S_0(v_i)$) of methane in its vibrational ground state (v=0) depends on the incident translational energy. For example for the dissociation of CH_4 on Ni(100) a nearly exponential rise in sticking coefficient is observed when the incident translational energy is increased from 10 to 100 kJ/mol[19].

Using IR laser pumping of the methane molecules incident on a metal surface it is possible to measure the quantum state resolved sticking coefficient for a specific vibrational state v_i. This is not simply found as the coverage divided by the dose from laser-on measurements, as the laser does not excite all of the molecules in the molecular beam, but only a fraction of the molecules (f_{exc}). There may also be vibrationally excited molecules in the beam due to the finite nozzle temperature even without laser excitation. The sticking coefficient obtained from 'laser-on' measurements ($S_0^{laser-on}$) includes contributions from molecules prepared in the state v_i by laser excitation, from thermally excited vibrations due to nozzle heating and from the molecules that remain in the vibrational ground state (v=0). The contribution that the thermally excited vibrations makes to the reactivity is identical with and without laser excitation as the laser only transfers molecules from v=0 to the vibrationally excited state v_i. It follows that $S_0(v_i)$ can be found using

$$S_0(v_i) = \frac{S_0^{laser-on} - S_0^{laser-off}}{f_{exc}} + S_0(0) \qquad (4)$$

where $S_0^{laser-off}$ is the sticking coefficient obtained without laser excitation and $S_0(0)$ is the sticking coefficient for molecules in v=0.

For a given vibrational state, v_i, the dependence of the sticking coefficient on kinetic energy can be fit with an S-shape curve[20]

$$S_0(v_i) = \frac{A(v_i)}{2}\left(1 + \mathrm{erf}\left|\frac{E_t - E_0^{v_i}}{W(v_i)}\right|\right) \qquad (5)$$

$A(v_i)$ is the asymptotic value of the sticking coefficient at high kinetic energy, $E_0^{v_i}$ is the average activation barrier for molecules in the vibrational state v_i, and $W(v_i)$ is the width of the distribution of barrier heights which can vary, for example, due to the different orientations the molecule can approach the surface in and different surface sites for the reaction. Fig. 15 shows an example of sticking coefficients for the dissociative chemisorption of methane on Ni(100) at a surface temperature (T_S) of 475 K for molecules with two quanta of antisymmetric stretch ($2v_3$) vibration added *via* laser excitation and for molecules without vibrational excitation (laser-off)[19]. The solid lines are fits to the vibrationally excited and vibrational ground states, where the data were fit using the equation given above.

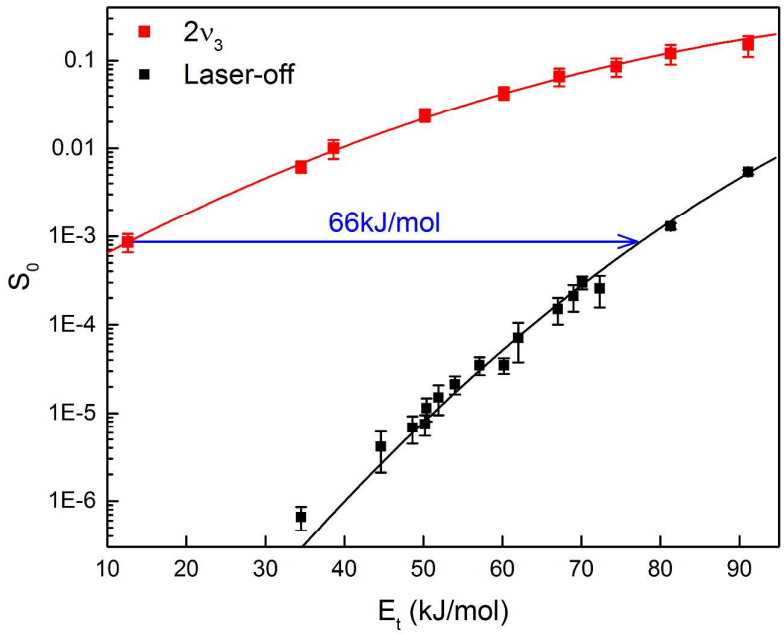

Fig. 15. The sticking coefficients measured for CH_4 molecules on a Ni(100) surface at a surface temperature of 475 K with two quanta of antisymmetric stretch ($2\nu_3$) vibration added through laser excitation and for vibrationally ground state molecules at a range of translational energies[19]. The solid lines show S-shape curve fits to the data, calculated using equation (5).

The extent to which vibrational energy promotes reactivity compared to translational energy is quantified by the vibrational efficacy, η^{ν_i}:

$$\eta^{\nu_i} = \frac{E_0^{v=0} - E_0^{\nu_i}}{E_{\mathrm{vib}}} \sim \frac{E_{\mathrm{t}}}{E_{\mathrm{vib}}} \qquad (6)$$

where $E_0^{v=0}$ and $E_0^{\nu_i}$ are determined by fitting S-shaped reactivity curves to the state resolved data keeping the fitting constants $A(\nu_i)$ and $W(\nu_i)$ the same for the different vibrational states, ν_i. Here, $E_0^{v=0} - E_0^{\nu_i}$ corresponds to the shift in translational energy between the state resolved reactivity curves. Adding 66 kJ/mol of translational energy increases $S_0(v{=}0)$ by the same amount as adding 72.1 kJ/mol of vibrational energy *via* the excitation of $2\nu_3$ state. From the data shown in Fig. 15 $\eta^{2\nu 3}$ = 0.9 indicating that the $2\nu_3$ vibration is less efficient than translation in promoting the chemisorption of CH_4 on Ni(100).

The vibrational efficacies provide a basis for comparison of the effect of different vibrational modes on the reactivity of methane. In a study of methane dissociation on Pt(110)[21] Bisson *et al.* prepared CH_4 in four different vibrationally excited eigenstates and measured the state resolved reactivity for each of these states as well as the laser-off reactivity. The data were again analysed by fitting S-shape reactivity curves of the form given above with identical $A(\nu_i)$ and $W(\nu_i)$ values in order to determine the value of $E_0^{\nu_i}$ for each state and the results used to calculate the vibrational efficacies for the four different vibrational states shown in table 1.

Normal mode	E_{vib}	E_t	η^{ν_i}
$\nu_1+\nu_4$ (stretch/bend)	50.6	33.9 ± 1.1	66.9 ± 2.1

$\nu_3+\nu_4$ (stretch/bend)	51.8	28.1 ± 1.2	54.3 ± 2.3
$2\nu_3$ (pure stretch)	72.1	33.6 ± 1.3	46.6 ± 1.8
$2\nu_2+\nu_4$ (pure bend)	52.2	20.9 ± 1.3	40.2 ± 2.6

Table 1. CH_4 vibrational normal mode, vibrational energy E_{vib} (kJ/mol), fitted shift along the kinetic energy axis E_t (kJ/mol) and calculated vibrational efficacy η^{ν_i} (%).

The fact that the vibrational efficacies are different for each of the four vibrational states of CH_4 shows that the methane reactivity is not simply a function of the total vibrational energy of the CH_4 molecule but depends on the identity of the reactant's quantum state. This is referred to as vibrational state (or mode) specificity. In an isolated gas molecule, the vibrational energy that is added to a specific vibrational eigenstate will remain localised in that state. However, as the molecule interacts with the surface, the vibration is not an eigenstate of the molecule-surface system. Instead, it can be expressed as a superposition of the eigenstates of the isolated molecule. The superposition state will have a time dependence which means that the initially localised vibrational energy can be transferred throughout the molecule. This process is referred to as surface induced intramolecular vibrational redistribution (IVR)[8]. The extent to which IVR occurs on the timescale of the collision will affect the relative reactivity of the different vibrational modes. The difference in vibrational efficacies demonstrates that the vibrational excitation remains localised in the initially prepared state, as opposed to being redistributed throughout the molecule through IVR. If IVR was complete, and the vibrational energy was randomised within the reactant molecule before the reaction occurred, the vibrational efficacy would be independent of the initially excited state.

While a number of state resolved experiments have explored the role of vibrational excitation in the dissociative chemisorption of methane on transition metal surfaces, there is only a single study to date which probes the effect of rotation on the methane dissociation probability[22]. Juurlink *et al.* [22] prepared CH_4 in the four lowest rotational levels of the ν_3 vibration and observed that rotational excitation does not change the reactivity of ν_3 excited CH_4 by more than a factor of two on Ni(100). This result may not seem surprising, considering the small amount of rotational energy E_{rot} relative to vibrational energy E_{vib} for these four states ($E_{rot} \leq 40$ cm^{-1} compared to $E_{vib} \cong 3000$ cm^{-1} of vibration) but it does exclude any strong effects on the CH_4 reactivity due to rotational hindering and dynamical steering[22].

4.2 Bond selectivity in gas-surface reactions

This section discusses how rovibrational excitation of the incident reactant molecule can be used to selectively break a specific bond in a chemisorption reaction with a surface, allowing different products to be formed depending on how the reactant was initially prepared. Being able to exert this level of control on the outcome of a gas-surface collision is of particular relevance for heterogeneous catalysis, where a specific reaction product may be favoured over other possible products. To investigate such bond selectivity experimentally it is necessary to be able to distinguish between the different

bonds of the molecule. For this, isotopic substitution is often used, for example, replacing hydrogen in methane with deuterium, as demonstrated below.

Killelea *et al.* first observed bond selectivity in a gas-surface reaction in the dissociative chemisorption of CHD_3 on a Ni(111) surface[23]. In CHD_3 chemisorption, either the unique C-H bond can break leaving CD_3 adsorbed on the surface plus an adsorbed H atom, or one of the three C-D bonds can break leaving CHD_2 and a D-atom adsorbed on the surface. Temperature programmed reaction of the adsorbates with subsurface D-atoms was used to quantify the adsorbed reaction products. For this technique, the surface temperature is increased linearly and desorbing species are detected by a mass spectrometer. For a Ni(111) surface it was previously shown by Johnson *et al.* that recombinative desorption of adsorbed methyl groups occurs exclusively with hydrogen atoms present in the bulk of the Ni crystal[24]. Bulk D-atoms were prepared by exposing the Ni(111) surface to a flux of D-atoms and subsequent bombardment of the surface with Xe-atoms. This causes recombinative desorption of surface bound D-atoms but leaves the subsurface D-atoms in place. As the surface temperature is increased to about 190 K, CHD_2 and CD_3 recombined with subsurface D-atoms, producing CHD_3 or CD_4 respectively. These would then desorb from the surface, and were detected by a mass spectrometer which monitored mass 19 (CHD_3) and mass 20 (CD_4). The ratio of the two signals could then be used to quantify the branching ratio of C-D to C-H bond cleavage. At higher kinetic energies they found that the branching ratio was 3:1, i.e for every C-H bond that broke, 3 C-D bonds would break, as would be expected statistically. At lower kinetic energies, the fraction of C-H bond cleavage was observed to be as high as 0.4, showing that at lower energies the less reactive C-D bond is less likely to break.

Having determined the branching ratio as a function of translational energy, Killelea *et al.* used IR pumping to excite the ν_1 normal mode of CD_3H, which corresponds to selective excitation of the C-H bond. The translational energy of the molecules in this case was chosen so that the total (vibrational + kinetic) energy was the same as the translational energy that led to the statistical branching ratio discussed above when the molecules were not vibrationally excited. This ensured that any differences in reactivity were not due to the total energy, but rather due to replacing incident kinetic energy with vibrational energy in the C-H bond. They found that the C-D to C-H branching ratio for the molecules excited to ν_1 was at least 1:30, *i.e.* the vibrationally excited C-H bond was at least 30 times more likely to break than a C-D bond. Therefore, selective excitation of the C-H bond increased the reactivity of the bond relative to the C-D bonds in CD_3H by a factor of at least 90.

Chen *et al.* extended the study of bond selectivity in methane chemisorption to all the partially deuterated methanes CH_3D, CD_2H_2 and CHD_3 for their chemisorption on Pt(111)[17]. In this work the surface bound dissociation products were detected using Reflection Absorption Infrared Spectroscopy (RAIRS), a more generally applicable technique which can distinguish the different adsorbed methyl species by their infrared absorption spectra, as shown in Fig. 16. The measurements showed that in the absence of vibrational excitation and with high incident kinetic energy, the branching ratio for C-H:C-D cleavage is near the statistical limit for each of the deuterated methanes with a slight preference for breaking the C-H bond.

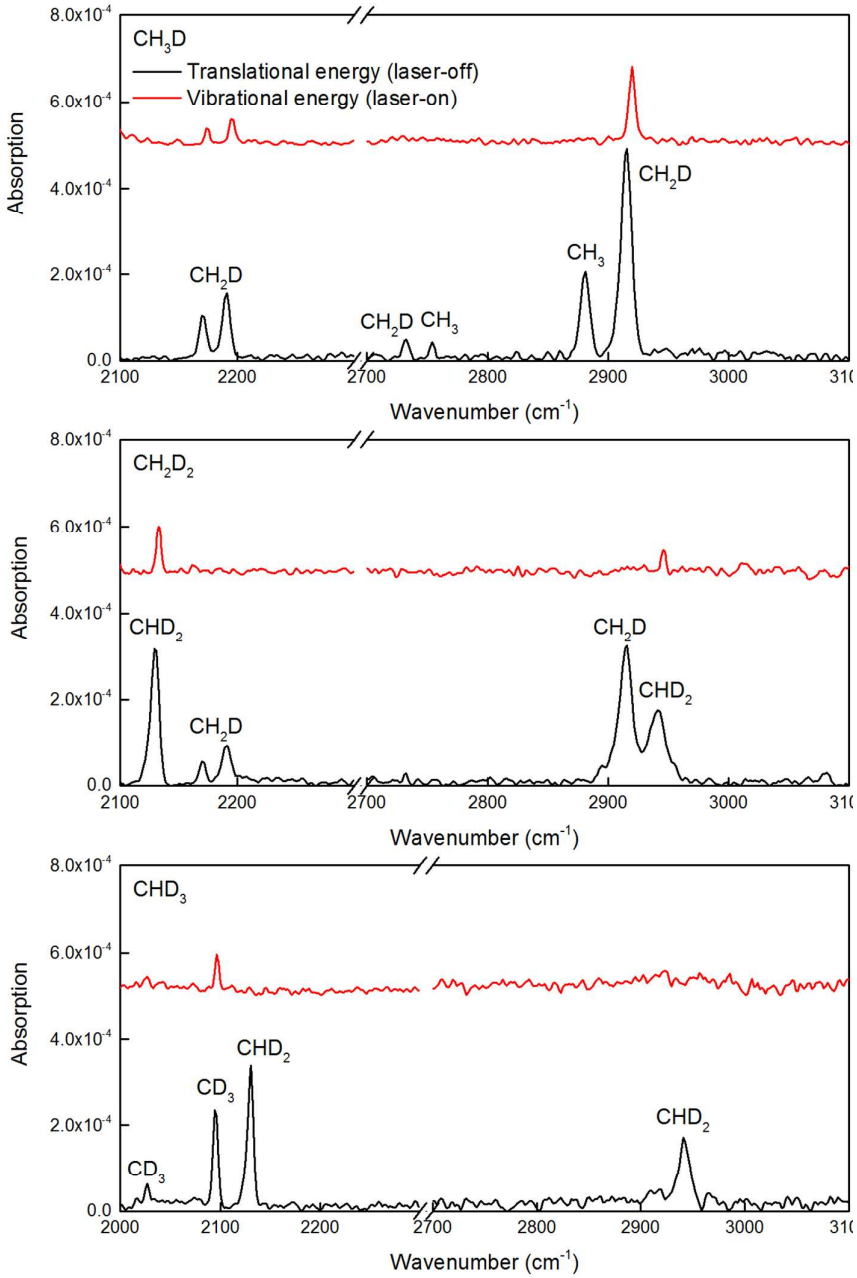

Fig. 16. RAIR spectra recorded following the dissociative chemisorption of CH_3D (top), CH_2D_2 (middle) and CHD_3 (bottom) on a Pt(111) surface. The black traces correspond to molecules with high kinetic energies (no laser excitation), and the red traces to C-H stretch vibrationally excited molecules.

Chen *et al.* then prepared each of the methane isotopologues with C-H stretch excitation and measured the state resolved branching ratios on Pt(111) using RAIRS. Compared to the laser-off measurements, the incident kinetic energy was reduced to keep the total energy of the molecules (kinetic + vibrational) the same as the translational energy for the laser-off measurements. For each of the deuterated methanes, only C-H bond cleavage was observed when the C-H stretch was vibrationally excited with the laser, with there being no detectable C-D cleavage, as shown by the red traces in Fig. 16.

Vibrational bond selectivity has been reported previously for bimolecular reactions in the gas phase by the groups of Crim[25, 26] and Zare[27]. For example, the outcome of the reaction of CH_3D with Cl-atoms could be controlled by vibrational excitation of the methane reagent. Preparation of CH_3D in the first overtone of the C-D stretch vibration led exclusively to CH_3 + DCl products. Conversely, excitation of either the symmetric or antisymmetric C-H stretch normal mode always led to C-H bond cleavage producing only CH_2D and HCl products. The observed bond selectivity could be rationalised by the fact that the prepared vibrational states contain a substantial amount of motion along the reaction co-ordinate of either C-H or C-D cleavage. The strong bond selectivity observed both in the gas phase and in gas-surface reactions confirms that the reaction is non-statistical and that IVR within the methane reagent is absent or incomplete on the timescale of the reactive collision. If IVR were complete, the vibrational energy that was initially located in the C-H stretch vibration would become delocalised throughout the molecule, and would promote reactivity of both the C-H and C-D bonds, leading to the observation of a statistical branching ratio.

4.3 Steric effects in chemisorption

The use of laser excitation not only allows the preparation of a reactant in a single excited rovibrational level in the molecular beam, but can also be used to create an anisotropic distribution of the molecules total angular momentum, ***J***. This additional level of control provides a method for probing the anisotropy of the molecule-surface interaction. Circularly polarised light can be used to create an initially oriented sample where the population of the +*m* levels is, for example, larger than that of the -*m* levels, where *m* is the projection of ***J*** onto the quantisation axis z. Classically an oriented sample corresponds to ***J*** pointing along the direction of the +z axis instead of the –z axis, as shown schematically in the left hand panel of Fig. 17. An aligned distribution can be prepared using linearly polarised light. Here, the population of the +|*m*| level is the same as that of the -|*m*| level but, for example, high |*m*| levels are preferentially populated over low |*m*| levels, as depicted in the right hand panel of Fig. 17. This corresponds classically to a distribution where ***J*** lies parallel to the z axis as opposed to perpendicular to it[28].

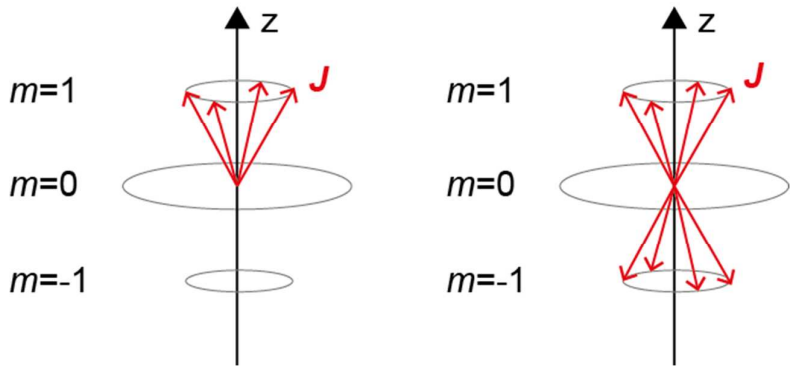

Fig. 17. A schematic representation of the anisotropic distribution of *m* levels that gives an oriented distribution (left) and aligned distribution (right) of ***J*** for *J*=1.

To probe for steric effects in a reaction it is necessary to create an initially oriented or aligned sample through laser excitation. This review will focus on creating alignment as this is most relevant for the discussion that follows. The selection rule for the absorption of a linearly polarised photon is $\Delta m=0$ and, for Q branch excitation only, $m\neq0$. A schematic representation of the allowed transitions for P, Q and R branch excitation is shown in Fig. 18. The magnitude of the alignment it is possible to create in each case depends on a number of factors including the value of *J* and the laser power used to excite the molecules. If a high laser power is employed such that the transition is saturated (referred to as strong pumping), or if rapid adiabatic passage is used, then either half or all of the population from the initial *m* level is transferred to the excited state. This means that the *m* levels in the final state which are populated through laser excitation have the same population if the initial distribution was isotropic in the ground state, whereas those not populated through laser excitation will have negligible population. It follows that in the strong pumping limit it is not possible to create an alignment using P branch excitation, as the population of each *m* level in the excited state is the same. Both R and Q branch excitation will create an initially aligned distribution, with ***J*** being aligned perpendicular to the laser polarisation following R branch excitation and aligned parallel to the laser polarisation following Q branch excitation. The magnitude of the alignment will decrease with increasing *J* in both cases. If a lower laser power (referred to as weak pumping) is used then the population transferred from the ground *m* level to the excited *m* level is proportional to the transition strength meaning it is possible to create alignment using P, Q or R branch excitation.

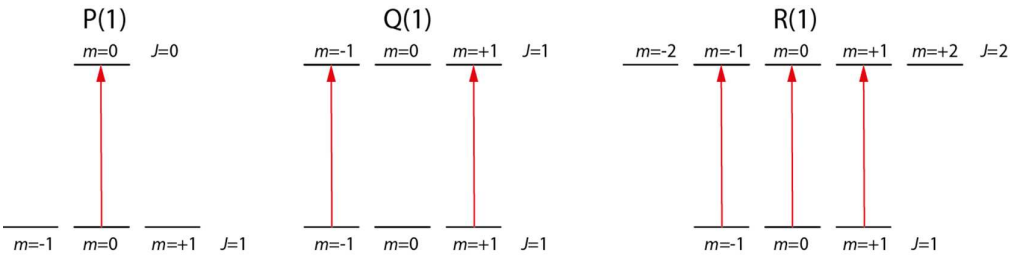

Fig. 18. An overview of the allowed transitions for P, Q and R branch excitation for the absorption of a linearly polarised photon.

Yoder *et al.* excited a single rovibrational state using linearly polarised light to create initially aligned samples of vibrationally excited CHD_3 molecules and investigated the alignment dependence of the chemisorption probability ($S_0(\theta)$) on a Ni(100) surface[29, 30], where θ is the angle between the laser polarisation and the plane of the surface. The aligned molecules were prepared through excitation of the C-H stretch normal mode ν_1 by linearly polarised IR light using RAP. Alignment of ***J*** also aligns the vibrational amplitude of the molecule which for CHD_3 lies along the unique C-H bond. When Q branch excitation is used, both ***J*** and the C-H bond are aligned parallel to the laser polarisation, and for R branch excitation the C-H bond is parallel and ***J*** perpendicular to the laser polarisation. Rotating the laser polarisation changes the alignment of both ***J*** and the incident C-H bond with respect to the plane of the surface. For R branch excitation, they found that the sticking coefficient

decreased as they rotated the laser polarisation from parallel to perpendicular to the surface, as shown in the left hand panel of Fig. 19. They observed that the reactivity when the laser polarisation was parallel to the surface (corresponding to 0° in Fig. 19) was up to 60% larger than when the laser polarisation was aligned perpendicular to the surface (90° in Fig. 19). They repeated the experiment using Q branch excitation, and obtained the same result with the reactivity being larger when the laser polarisation was parallel to the surface than perpendicular to the surface. As the direction of the vibrational amplitude is parallel to the laser polarisation in both cases, but the direction of ***J*** is parallel to the polarisation for Q branch excitation and perpendicular for R branch excitation, this demonstrates that the alignment effect is not due to the alignment of ***J*** but due to the alignment of the vibrational amplitude.

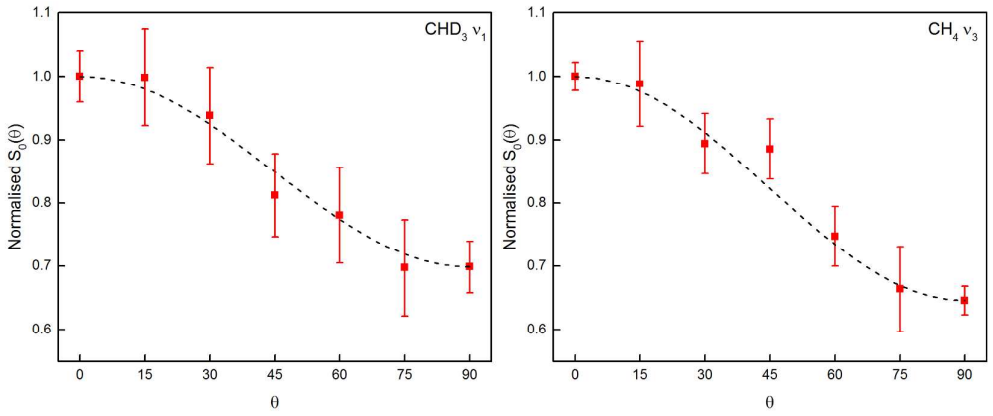

Fig. 19. The sticking coefficient, normalised to the value measured when the laser polarisation was parallel to the surface ($S_0(\theta)$) as a function of the angle between the laser polarisation and the surface (θ) for CHD_3 following ν_1 excitation (left) and CH_4 following ν_3 excitation (right). The points correspond to experimental data obtained following R(0) excitation, and the line shows the trend in the data.

Yoder *et al.* also studied the alignment dependence of the dissociative chemisorption of $CH_4(\nu_3)$ on Ni(100), where ν_3 corresponds to the antisymmetric C-H stretch normal mode. The ν_3 mode imparts the same C-H stretch amplitude to all four bonds of the CH_4, only the relative phase of the stretch vibrations differ. Therefore, ν_3 excitation does not align any specific C-H bond, it only aligns the vibrational amplitude of the molecule parallel to the laser polarisation. Again it was observed that the dissociation probability was largest when the laser polarisation was parallel to the surface and smallest when the polarisation was along the surface normal, as shown in the right hand panel of Fig. 19. The same trend was obtained for both Q and R branch excitation, confirming that the observed effect is not due to alignment of a single C-H bond but is due to the alignment of the vibrational amplitude of the methane.

The dependence of the reactivity on the alignment of the vibration demonstrates the absence of strong steering effects as the molecule approaches the surface. These would 'steer', or rotate, the molecules along the minimum energy path towards the most favoured transition state geometry irrespective of how the initial ensemble of molecules was prepared. If this was the case, the

reactivity of the molecules should be independent of whether the alignment of the vibrational amplitude is parallel or perpendicular to the surface. The change in reactivity as the laser polarisation is rotated shows that the molecules do not necessarily follow the minimum energy path across the PES, which is often assumed to be the case in theoretical models of gas-surface interactions.

4.4 Vibrationally state resolved studies of physisorption

The results presented so far have all focussed on the dissociative chemisorption of molecules on surfaces, where a bond is broken within the molecule and new bonds are formed between the fragments and the surface. As has been demonstrated, the dissociative chemisorption of methane is enhanced by adding vibrational energy to the molecules *via* laser excitation. However, less is known about how vibrational excitation affects the probability of trapping molecular methane on transition metal surfaces. Chen *et al.* used RAIRS to compare the trapping probability of $CH_4(v=0)$ and $CH_4(\nu_3)$ on a Pt(111) surface at a temperature (T_S) of 77 K and found no detectable change in trapping probability due to excitation of the antisymmetric C-H stretch normal mode ν_3 of the incident methane[31]. The RAIR spectra recorded with and without laser excitation are shown in Fig. 20.

At T_S=77 K , the desorption lifetime of CH_4(ads) was measured to be on the order of 0.25 sec which leads to a dynamic equilibrium between the incident molecular beam flux and the flux that thermally desorbs from the surface. This results in a steady state CH_4(ads) coverage of 0.05 monolayers as monitored by the RAIRS absorption signal. Any change in the trapping probability due to excitation of the ν_3 vibration in the incident methane beam should result in a change in the steady state coverage if the desorption lifetime is not affected by the vibrational excitation (see below). The fact that there was no detectable change in the RAIRS absorption signal for a beam of pure $CH_4(v=0)$ and a beam in which 30% of the incident beam is excited to the ν_3 vibration indicates that the trapping probability of $CH_4(v=0)$ and $CH_4(\nu_3)$ are identical within the detection limit of the experiment.

Analogous results have been observed in other systems, for example the Wodtke group has studied the trapping of NO on Au(111) and found that the trapping probability remains unchanged when two quanta of vibration are added to the incident NO[32]. Also the trapping of D_2O on ice was found to be unaffected by vibrational excitation of the incident D_2O[33].

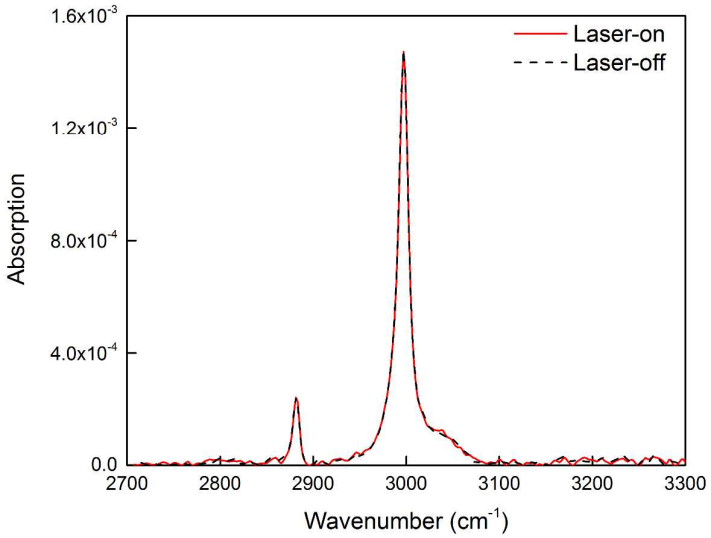

Fig. 20. A comparsion of the RAIR spectra of rovibrationally excited methane (red solid line) and ground state methane (dashed black line) physisorbed on a Pt(111) at a surface temperature of 77 K.

The independence of the physisorption probability on vibrational excitation of the incident molecules is in marked contrast to the dissociative chemisorption results presented earlier in this review, where rovibrational excitation increases the probability that the molecule dissociatively chemisorbs on the surface. The results indicate that vibrational to translational (V-T) energy transfer is inefficient during the molecule-surface interaction and that the vibration acts as a spectator to the collision. If V-T energy transfer was efficient, the trapping probability would be expected to decrease when the incident molecule is vibrationally excited. Sibener and Lee have studied the trapping of CCl_4 and SF_6 trapping on their respective solid phases and found evidence for a decrease in trapping probability upon vibrational excitation[34]. In these experiments low frequency vibrational modes were populated by thermal activation of the beam using a hot nozzle rather than IR laser pumping. For these lower frequency vibrations V-T transfer is expected to be more efficient due to a smaller vibrational energy gap.

Further evidence that vibration acts as a spectator and remains localised in the molecule when it traps is provided by a recent study by Utz *et al.* for the dissociative chemisorption of methane on Ir(111)[35]. They observed that the sticking coefficient decreased as the incident translational energy of the methane increased between 2 kJ/mol and 10 kJ/mol for both laser-off and laser-on measurements. As discussed above, this decrease with increasing kinetic energy is characteristic of the methane being initially trapped in a precursor state before the dissociation reaction occurs. The fact that vibrational excitation still promotes the dissociative chemisorption of molecules that are initially trapped suggests that the energy remains localised in the molecule rather than being transferred to the surface, where it would no longer be available to surmount the activation barrier. It also suggests that the laser excitation does not affect the trapping probability into the initial precursor state.

If trapping is insensitive to vibrational excitation, it would be expected that the reverse process of desorption of a physisorbed molecule from a surface is also not affected by vibrational excitation of the adsorbed molecule. Numerous

attempts to perform direct resonant desorption of physisorbed molecules have been described in the literature but without success[36, 37]. If direct resonant desorption were feasible it could be used to perform laser isotope separation where only the laser excited isotope would desorb from a physisorbed mixture of isotopologues. However, when desorption was detected due to vibrational excitation of a physisorbed species it was always found to be due to a thermal process causing simultaneous desorption of all isotopologues through substrate heating by vibrational energy transfer from the adsorbed molecules to the surface.

5. Comparison of quantum state resolved data to theory

The quantum state resolved gas-surface reactivity data obtained by the experiments described in this review are ideally suited for comparison with the predictions of different theoretical models for gas-surface reactions since there is no need for extensive averaging over rotational and vibrational quantum states. Several examples of such comparisons are briefly described, which have been useful in guiding the development of the theory of gas-surface reactivity.

5.1 A statistical model for chemisorption

A statistical model for the chemisorption reaction of methane on Pt(111) was developed by the group of Harrison[38]. The so-called PC-MURT model (Physisorbed Complex Microcanonical Unimolecular Rate Theory) assumes that the incident methane molecule forms a transient physisorbed complex with several surface atoms before the dissociation reaction occurs. It is further assumed that rapid vibrational energy redistribution (IVR) within the physisorbed complex completely randomises the initial internal energy of the incident methane before dissociation occurs. The dissociation rate is calculated using Rice-Ramsberger-Kassel-Marcus (RRKM)[39, 40] theory. The model includes three fitting parameters which are the number of surface atoms in the complex, a single common phonon frequency for the surface oscillators, and the apparent energy barrier for the dissociation reaction. These parameters were adjusted to fit the predictions of the model to available experimental data from molecular beam and thermal reactivity measurements. More recently, Harrison *et al.* have extended the PC-MURT model to allow energy to be transferred between the precursor complexes and the surface[41], as well as to include the effects of tunneling through the activation barrier[42]. The resulting theory is referred to as the precursor mediated microcanonical trapping model (PMMT). While the PC-MURT and PMMT models are able to reproduce the measured sticking coefficients reasonably well, this cannot be interpreted as proof that the microscopic reaction mechanism is in fact statistical. The observation of state specificity, bond selectivity as well as the steric effects in the state resolved experiments described above are clear evidence that methane chemisorption is non-statistical and that the reaction rate does not simply depend on the total available energy but also on the initial quantum state and the alignment of the reactants. Therefore a dynamical theory is needed to predict methane chemisorption correctly at a microscopic level.

5.2 Dynamical models for methane chemisorption

A full dynamical theory of chemisorption should take into account all the degrees of freedom of the molecule-surface system. A methane molecule incident on a surface is fully specified by 3 translations, 3 rotations and 9 vibrations, leading to a 15 dimensional PES. While many groups have calculated PESs with reduced dimensionality ranging from 3 to 12 dimensions, the first principles calculation of a global 15 dimensional PES for methane on a transition metal surface using density functional theory (DFT) currently approaches the limits of computing power. Therefore the common strategy has been to limit the PES to the degrees of freedom considered to be relevant for the reaction such as C-H stretch vibrations and to calculate points of the PES along the minimum energy path (MEP) from reactants to products. For example, Halonen[43] *et al.* used a London Eyring Polanyi Sato (LEPS) surface fitted to spectroscopic data in combination with a 4 dimensional model which includes only the C-H stretching modes of a CH_4 molecule incident onto a structureless surface. They calculated the normal modes of CH_4 under the influence of the molecule surface interaction for a range of distances from a metal surface for a fixed orientation with one of the C-H bonds pointing down towards the surface. By connecting the eigenstates in the order of their energy they obtain vibrationally adiabatic curves that can be used to predict the dynamics as the methane molecules approach the surface. They found that the initial excitation of the symmetric C-H stretch mode ν_1 far from the surface is transformed by the interaction with the surface into a localised stretching of the C-H bond pointing towards the surface. On the other hand, if the antisymmetric ν_3 mode is excited far from the surface this surface-induced IVR causes the C-H stretch amplitude to be quarantined in the CH_3 group pointing away from the surface. Based on the opposing localisation of the C-H stretch amplitude for the ν_1 and ν_3 modes, Halonen *et al.* predicted that the ν_1 mode should be more efficient in activating the dissociative chemisorption of CH_4 than the ν_3 mode, which was later confirmed by state resolved reactivity measurements for $CH_4(\nu_1)$ and $CH_4(\nu_3)$ for the dissociation on a Ni(100) surface[44].

Quantitative predictions of methane reactivity on transition metal surfaces require a more realistic multidimensional PES on which either classical dynamics or quantum dynamics calculations can be performed. A number of theory groups have calculated PESs for motion along the MEP for methane chemisorption ranging from 3 to 15 dimensions. The most important part of the PES lies in the vicinity of the MEP from reactants to products which crosses the transition state at the top of the barrier. Fig. 21 shows four snapshots of a CH_4 molecule moving along this MEP on a 15 dimensional PES which was calculated along the MEP from work by the Kroes group[45]. The transition state (TS) shown in (c) has the dissociating C-H bond significantly stretched from the gas-phase value (1.588 Å vs 1.09 Å) and bent away from the tetrahedral angle (79.8° vs 109.4°)

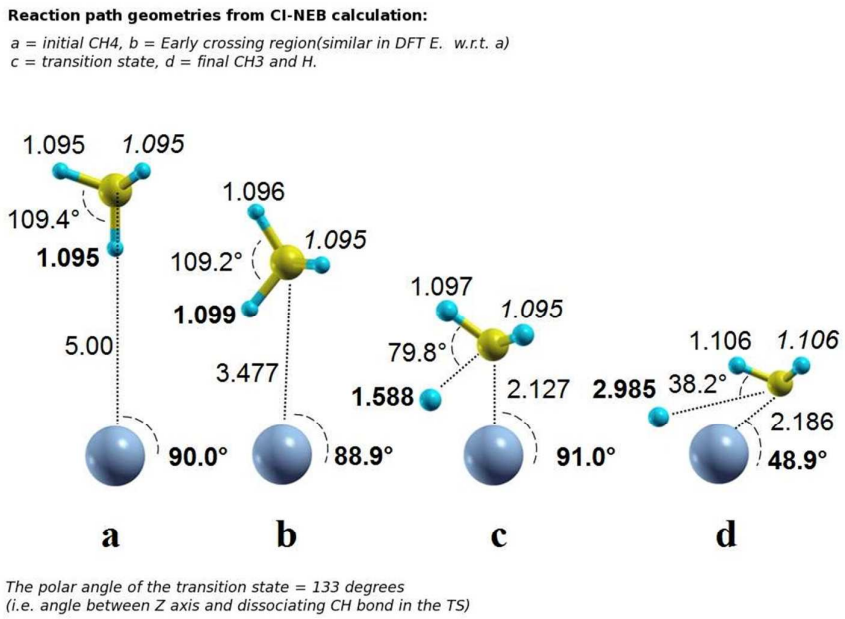

Fig. 21. Calculated representation of a methane molecule moving along the MEP towards dissociation on Ni(111). Reproduced from Ref. [45] with permission from the PCCP Owner Societies.

Comparison of the TS structure with the initially prepared vibrational state of CH_4 offers an intuitive explanation for the vibrational state specificity observed in the state resolved experiments. Preparation in a vibrational state which distorts the CH_4 molecules towards the structure of the TS, will move the system along the reaction path and should therefore be more efficient in activating the dissociation than any state of similar vibrational energy but with little resemblance to the TS. The so-called sudden vector projection (SVP) model proposed by Hua Guo quantifies this resemblance between the initial vibrational state and the TS structure by calculating the overlap (projection) between the two states and relating the overlap to the observed vibrational efficacy[46, 47]. The model is called 'sudden' because it neglects any surface induced IVR by assuming that the reactive collision time is much shorter than the time needed for any significant IVR to occur.

A detailed dynamical treatment for methane dissociation on transition metals including surface induced IVR was developed by the group of Bret Jackson.[48, 49] His so-called reaction path model first calculates the MEP connecting reactants and products in 15 dimensions using DFT. For simplicity, the PES is assumed to be harmonic in the 14 dimensions orthogonal to the MEP. The reaction dynamics are then calculated by propagating wavepackets, corresponding to one of the possible initial vibrational states on the PES. Fig. 22 shows how the frequency of the 9 vibrational normal modes of CH_4 changes as the molecule approaches a Ni(100) surface along the reaction path. The symmetric C-H stretch mode ν_1 is found to soften more than the antisymmetric C-H stretch mode ν_3 and the bending modes ν_2 and ν_4. This mode softening leads to a lowering of the activation barrier along the vibrationally adiabatic reaction channels which is largest for the ν_1 mode consistent with the highest vibrational efficacy observed experimentally for this mode.

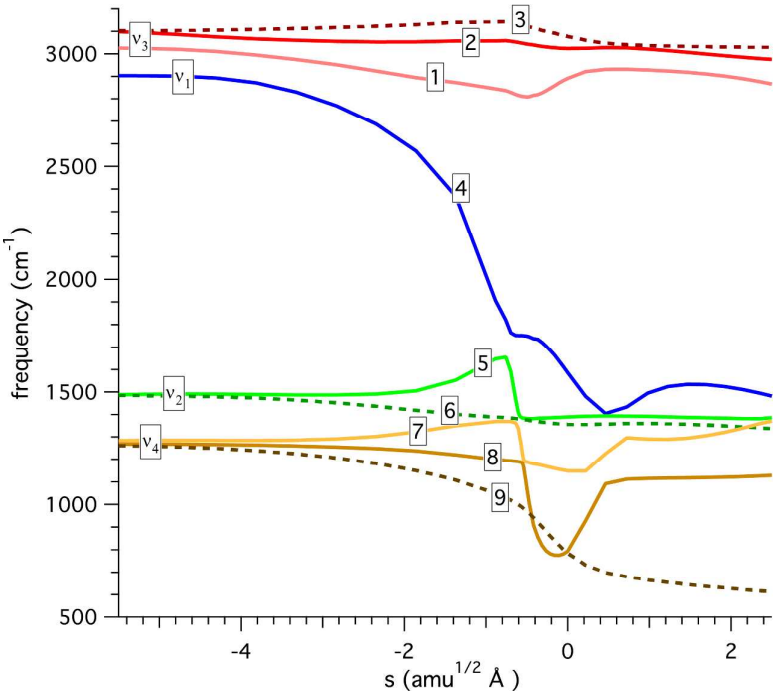

Fig. 22. The change in frequency of the 9 vibrational normal modes of methane as the molecule approaches the surface along the reaction path (denoted s in the figure).[48]

The quantum mechanical propagation includes the possibility of transitions between the different vibrational states due to non-adiabatic couplings that arise from the molecule-surface interaction. Transitions to states of lower energy convert vibrational energy into translation along the reaction path, which increases the reactivity. For reasons of symmetry not all the vibrational states can undergo transitions to the ground state and for the others the non-adiabatic couplings to the ground state are state specific. Therefore the non-adiabatic transitions contribute to the reactivity enhancement due to the initial vibrational excitation in a state specific way.

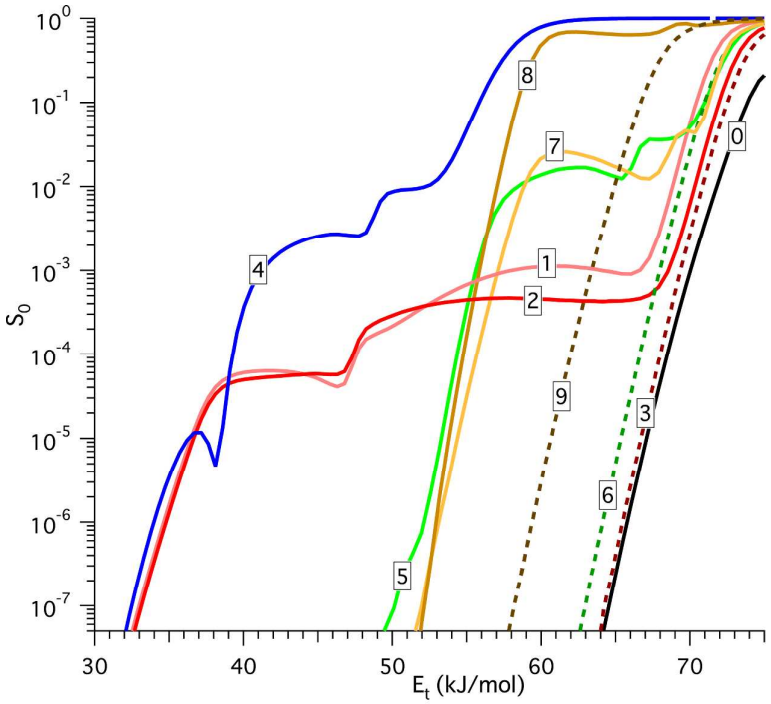

Fig. 23. The sticking coefficient as a function of translational energy for the 9 normal modes of methane (1-9) as well as the ground state (0) calculated using the RPH model.[48]

Fig. 23 shows the sticking coefficient S_0 as a function of incident translational energy E_t for the 9 normal modes of CH_4 and the vibrational ground state as calculated by the Reaction Path Hamiltonian (RPH) model for dissociation on a flat rigid Ni surface. The structures in some of the vibrationally adiabatic sticking curves can be explained as follows: With decreasing translational energy, S_0 drops when E_t drops below the vibrationally adiabatic barrier. For states 1 and 2 which belong to the ν_3 mode this drop occurs near E_t=75 kJ/mol, whereas for the ν_1 mode labelled 4 in the figure the drop is shifted down to E_t=60 kJ/mol due to the reduced barrier height caused by the strong mode softening for the ν_1 mode. The remaining reactivity is due to non-adiabatic transitions to the ground state which for the ν_1 mode liberates sufficient energy along the reaction path that the reactivity stays above 10^{-3} for E_t>40 kJ/mol.

Taken together, the RPH model explains the experimentally observed mode specific reactivity of CH_4 due to differences in the mode softening and the nonadiabatic couplings to vibrational states of lower energy for the different initial vibrationally excited states.

The theoretical methods discussed above start with the calculation of a PES followed by either classical or quantum mechanical simulation of the reaction dynamics on the calculated PES. An alternative method for theoretical calculations is to model the interaction using *ab initio* molecular dynamics (AIMD) calculations. This method uses first principles electronic structure calculations to calculate the forces acting on the molecule and the surface throughout the reaction 'on the fly'. In this way only regions of the PES which are sampled along the reaction path have to be calculated which makes it possible to include all the molecular degrees of freedom as well as those of several layers of surface atoms. It follows that AIMD calculations provide a tool to test and

validate the approximations made in the theoretical calculations discussed above.

Nattino *et al.* used AIMD calculations to study the dissociative chemisorption of CD_3H on Pt(111)[50]. They used quasiclassical trajectory methods to propagate the motion of the molecule and the surface, where the 'quasi' refers to the fact that some quantum mechanical effects are included in the calculations, in this case referring to the inclusion of vibrational zero point energy. The results of the calculation overestimated the laser off sticking coefficients, suggesting that the activation barrier is too low. They also provided insight into the validity of sudden approximations that are often employed in theoretical calculations. Firstly, it was demonstrated that there was a lack of translational steering of the molecule towards reactive sites in the plane parallel to the surface, supporting the use of sudden approximations for describing the translational motion of the molecule in this plane. This approximation is often used, with the final sticking coefficient calculated as the average of the sticking coefficients for different surface sites. Secondly, it was shown that there was no rotational steering of the molecule towards the minimum energy path as it approached the surface, suggesting that the use of rotationally sudden approximations in calculations are also valid. This conclusion is also supported by the stereospecificity of the dissociative chemisorption of methane on transition metal surfaces discussed above.

Summary and outlook

This review has shown how quantum state resolved reactivity measurements can help to untangle the complicated nature of dynamics at the gas-surface interface. Experiments have been employed which couple molecular beams with laser excitation through rapid adiabatic passage, which can be used to transfer all the population from an initial rovibrational level to a final rovibrational level. This can be done for single or double resonance excitation, increasing the number of vibrational states and modes that can be prepared. The sticking coefficient or trapping probability can then be determined using King and Wells measurements, Auger Electron Spectroscopy or Reflection Absorption Infrared Spectroscopy, with the choice of detection method depending on the size of the adsorption probability being measured and the effect being investigated. AES is the most widely applicable technique for quantifying the adsorbates on the surface, but RAIRS also provides structural information on the adsorbates and can be used in-situ and online to record an uptake curve in a single experiment.

The main focus has been on the effect of vibrational excitation on the trapping and sticking of methane on transition metal surfaces. The dependence of these two processes on vibrational excitation is markedly different, with excitation having no observable effect on the trapping probability whereas vibrational excitation promotes dissociative chemisorption. The observed reactivity enhancement demonstrates that chemisorption of methane is state specific. Using partially deuterated methanes, it has also been shown that by adding vibrational excitation to the C-H stretching modes, a C-H bond can be selectively broken instead of a C-D bond, demonstrating bond selectivity. Excitation by linearly polarised radiation enables the preparation of a beam of

aligned methane which was used to show that methane chemisorption depends on the alignment of the vibrational amplitude relative to the surface. The observed vibrational state specificity, bond selectivity and stereospecificity all demonstrate the highly non-statistical nature of the chemisorption of methane on transition metal surfaces. Despite these complexities, detailed first principles calculations have been developed that successfully capture these trends, helping towards the goal of achieving a predictive understanding of the gas-surface interaction.

The state resolved experiments described in this review have focused on the dissociative sticking of methane on a transition metal surface leading to chemisorbed products, or the molecular trapping of methane leading to physisorbed products. However, for the beam/surface experiments described above, the majority of the incident methane molecules do not dissociate but are scattered from the surface back into the gas phase. Little is known about the extent of vibrational and rotational energy transfer in a methane collision with a transition metal surface. This scarcity of state resolved information about methane scattering is mainly due to a lack of a scheme for the state specific detection of scattered methane by resonant multiphoton ionisation (REMPI). We recently developed a quantum state resolved detection method for surface scattered methane using a combination of state specific infrared laser tagging with a highly sensitive cryogenically cooled bolometer. This method enables us to perform state-to-state surface scattering experiments which explore in detail the vibrational and rotational energy transfer in methane-surface scattering as well as the extent of surface induced vibrational energy redistribution. These measurements, which are currently being undertaken in our laboratory, will complement those presented in this review, provide a further stringent test of the theoretical calculations and increase our understanding of interactions at the gas-surface interface.

Acknowledgements

We gratefully acknowledge financial support provided by the Swiss National Science Foundation (Grant No. 159689/1) and the Ecole Polytechnique Fédérale de Lausanne as well as the important contributions of doctoral students Mathieu Schmid, Plinio Maroni, Tung T. Dang, Marco Sacchi, Bruce L. Yoder, Li Chen, Morten Hundt, Maarten van Reijzen, Jörn Werdecker and Ana Gutiérrez, and of postdoctoral associates Régis Bisson and Hirokazu Ueta at the EPFL.

References

1. D. R. Killelea, V. L. Campbell, N. S. Shuman, R. R. Smith and A. L. Utz, *The Journal of Physical Chemistry C*, 2009, **113**, 20618-20622.
2. A. L. Utz, *Current Opinion in Solid State and Materials Science*, 2009, **13**, 4-12.
3. R. D. Beck and A. L. Utz, in *Dynamics of Gas-Surface Interactions Atomic-level Understanding of Scattering Processes at Surfaces*, eds. R. Dâiez Muiäno and H. F. Busnengo, Springer, Berlin, 2013.
4. R. I. Masel, *Principles of adsorption and reaction on solid surfaces*, Wiley, New York etc., 1996.
5. P. Kisliuk, *Journal of Physics and Chemistry of Solids*, 1957, **3**, 95-101.
6. P. Kisuuk, *Journal of Physics and Chemistry of Solids*, 1958, **5**, 78-84.

7. G. Scoles, *Atomic and molecular beam methods*, Oxford University Press, New York etc., 1988.
8. D. R. Killelea and A. L. Utz, *Physical Chemistry Chemical Physics*, 2013, **15**, 20545-20554.
9. X.-G. Wang and E. L. Sibert, *The Journal of Chemical Physics*, 1999, **111**, 4510-4522.
10. H. Chadwick, P. M. Hundt, M. E. van Reijzen, B. L. Yoder and R. D. Beck, *The Journal of Chemical Physics*, 2014, **140**, 034321.
11. P. M. Hundt, M. E. van Reijzen, H. Ueta and R. D. Beck, *The Journal of Physical Chemistry Letters*, 2014, **5**, 1963-1967.
12. P. Maroni, D. Papageorgopoulos, A. Ruf, R. D. Beck and T. R. Rizzo, *Review of Scientific Instruments*, 2006, **77**, 054103.
13. D. A. King and M. G. Wells, *Surface Science*, 1972, **29**, 454-482.
14. M. P. Schmid, P. Maroni, R. D. Beck and T. R. Rizzo, *Review of Scientific Instruments*, 2003, **74**, 4110-4120.
15. L. Vattuone, Y. Y. Yeo, R. Kose and D. A. King, *Surface Science*, 2000, **447**, 1-14.
16. L. Chen, H. Ueta, R. Bisson and R. D. Beck, *Review of Scientific Instruments*, 2013, **84**, 053902-053909.
17. L. Chen, H. Ueta, R. Bisson and R. D. Beck, *Faraday Discussions*, 2012, **157**, 285-295.
18. J. C. Polanyi, *Accounts of Chemical Research*, 1972, **5**, 161-168.
19. M. P. Schmid, P. Maroni, R. D. Beck and T. R. Rizzo, *The Journal of Chemical Physics*, 2002, **117**, 8603-8606.
20. L. B. F. Juurlink, D. R. Killelea and A. L. Utz, *Progress in Surface Science*, 2009, **84**, 69-134.
21. R. Bisson, M. Sacchi and R. D. Beck, *Physical Review B*, 2010, **82**, 121404.
22. L. B. F. Juurlink, R. R. Smith and A. L. Utz, *Faraday Discussions*, 2000, **117**, 147-160.
23. D. R. Killelea, V. L. Campbell, N. S. Shuman and A. L. Utz, *Science*, 2008, **319**, 790-793.
24. A. D. Johnson, S. P. Daley, A. L. Utz and S. T. Ceyer, *Science*, 1992, **257**, 223-225.
25. S. Yoon, R. J. Holiday and F. F. Crim, *The Journal of Physical Chemistry B*, 2005, **109**, 8388-8392.
26. C. J. Annesley, A. E. Berke and F. F. Crim, *The Journal of Physical Chemistry A*, 2008, **112**, 9448-9453.
27. Z. H. Kim, H. A. Bechtel and R. N. Zare, *Journal of the American Chemical Society*, 2001, **123**, 12714-12715.
28. A. J. Orr-Ewing and R. N. Zare, *Annual Review of Physical Chemistry*, 1994, **45**, 315-366.
29. B. L. Yoder, R. Bisson and R. D. Beck, *Science*, 2010, **329**, 553-556.
30. B. L. Yoder, R. Bisson, P. M. Hundt and R. D. Beck, *The Journal of Chemical Physics*, 2011, **135**, 224703-224709.
31. L. Chen, H. Ueta, H. Chadwick and R. D. Beck, *The Journal of Physical Chemistry C*, 2014, DOI: 10.1021/jp5064897.
32. A. M. Wodtke, H. Yuhui and D. J. Auerbach, *Chemical Physics Letters*, 2005, **413**, 326-330.

33. P. M. Hundt, R. Bisson and R. D. Beck, *The Journal of Chemical Physics*, 2012, **137**, 074701-074706.
34. S. J. Sibener and Y. T. Lee, *The Journal of Chemical Physics*, 1994, **101**, 1693-1703.
35. E. Dombrowski, E. Peterson, D. Del Sesto and A. L. Utz, *Catalysis Today*, 2015, **244**, 10-18.
36. T. J. Chuang, H. Seki and I. Hussla, *Surface Science*, 1985, **158**, 525-552.
37. B. Redlich, H. Zacharias, G. Meijer and G. von Helden, *The Journal of Chemical Physics*, 2006, **124**, 044704.
38. V. A. Ukraintsev and I. Harrison, *The Journal of Chemical Physics*, 1994, **101**, 1564-1581.
39. R. A. Marcus, *The Journal of Chemical Physics*, 1952, **20**, 359-364.
40. P. J. Robinson and K. A. Holbrook, *Unimolecular reactions*, Wiley-Interscience, London, 1972.
41. S. B. Donald and I. Harrison, *Physical Chemistry Chemical Physics*, 2012, **14**, 1784-1795.
42. S. B. Donald, J. K. Navin and I. Harrison, *The Journal of Chemical Physics*, 2013, **139**, 214707.
43. L. Halonen, S. L. Bernasek and D. J. Nesbitt, *The Journal of Chemical Physics*, 2001, **115**, 5611-5619.
44. P. Maroni, D. C. Papageorgopoulos, M. Sacchi, T. T. Dang, R. D. Beck and T. R. Rizzo, *Physical Review Letters*, 2005, **94**, 246104.
45. K. G. Prasanna, R. A. Olsen, A. Valdes and G.-J. Kroes, *Physical Chemistry Chemical Physics*, 2010, **12**, 7654-7661.
46. B. Jiang, R. Liu, J. Li, D. Xie, M. Yang and H. Guo, *Chemical Science*, 2013, **4**, 3249-3254.
47. H. Guo and B. Jiang, *Accounts of Chemical Research*, 2014, **47**, 3679-3685.
48. S. Nave and B. Jackson, *Physical Review B*, 2010, **81**, 233408.
49. S. Nave, A. K. Tiwari and B. Jackson, *The Journal of Physical Chemistry A*, 2014, **118**, 9615-9631.
50. F. Nattino, H. Ueta, H. Chadwick, M. E. van Reijzen, R. D. Beck, B. Jackson, M. C. van Hemert and G.-J. Kroes, *The Journal of Physical Chemistry Letters*, 2014, **5**, 1294-1299.